ARPHA Preprints

PENSOFT

PREPRINT

Author-formatted, not peer-reviewed document posted on 29/04/2025

DOI: https://doi.org/10.3897/arphapreprints.e156971

Diverse metabolites with anti-psoriasis potential from different fermentations of the fungicolous fungus *Xylaria longipes* HFG1018

Zhen-Zhu Zhao, Yan Wang, Xiao-Yu Wang, Hui Chen, Zhen-Zhen Wang, Jing-Kun Wang, Le-Le Wang, Ming-Jun Shen, Xin Pang, Wei-Sheng Feng

ARPHA Preprints *Author-formatted, not peer-reviewed document posted on 29/04/2025.* DOI: https://doi.org/10.3897/arphapreprints.e156971

Diverse metabolites with anti-psoriasis potential from different fermentations of the fungicolous fungus *Xylaria longipes* HFG1018

Zhen-Zhu Zhao[1], Yan Wang[1], Xiao-Yu Wang[2], Hui Chen[1], Zhen-Zhen Wang[2], Jing-Kun Wang[1], Le-Le Wang[1], Ming-Jun Shen[1], Xin Pang[1]*, Wei-Sheng Feng[1]*

[1] School of Pharmacy, Henan University of Chinese Medicine, Zhengzhou 450046, China

[2] Academy of Chinese Medical Sciences, Henan University of Chinese Medicine, Zhengzhou 450046, China

Correspondence:

*Xin Pang, Email: pangxin116@163.com

*Wei-Sheng Feng, Email: fwsh@hactcm.edu.cn

ARPHA Preprints *Author-formatted, not peer-reviewed document posted on 29/04/2025.* DOI: https://doi.org/10.3897/arphapreprints.e156971

Abstract

The genus *Xylaria* is a promising source of bioactive compounds. This study explored the diversity of secondary metabolites (SMs) in *Xylaria longipes* under three fermentation conditions, isolating 14 new SMs and 27 known ones. The structures were elucidated using NMR, HRESIMS, ROESY, and *J*-based configuration analysis, with absolute configurations determined through calculated ECD and ^{13}C NMR data. A comprehensive library of SMs was constructed, facilitating metabolomics-wide association studies that identified culture conditions as a critical factor influencing SM production. This compound library also simplifies the determination of absolute configurations for diplosporins by analyzing *J* values and CD trends. Anti-proliferative assays against induced T/B lymphocytes and HaCaT cells revealed that more than half of the compounds exhibited significant inhibitory activity, with compounds **2**, **15**, and **32** reducing IFN-γ secretion. Compound **32** showed promising anti-psoriatic effects by inhibiting NF-κB p65 phosphorylation in HaCaT cells. This first systematic chemical study of *X. longipes* under varied conditions provides insights into structure-activity relationships.

Keywords: *Xylaria longipes*, Xylariaceae, Different fermentation conditions, Chemical investigation; Immunosuppression; HaCaT cells; Psoriasis

Introduction

Fungi of the genus *Xylaria* are predominantly saprophytic, with a minority exhibiting parasitic behavior. They thrive in forest ecosystems, often near ant colonies or forming symbiotic relationships with plants. These unique ecological niches endow *Xylaria* species with distinct characteristics (Chen et al., 2024). Research has identified terpenoids (Chen et al., 2020, 2024), sterols (Chen et al., 2024), alkaloids (Chen et al., 2024), cyclopeptides (Chen et al., 2024; Li et al., 2011; Wu et al., 2011), and polyketides (Chen et al., 2024; Masahiko et al., 2014; Ibrahim et al., 2014) as the primary chemical constituents produced by *Xylaria* species. Pharmacological studies have demonstrated that extracts or compounds derived from *Xylaria* exhibit a wide range of biological activities, including antioxidant, antibacterial, antitumor, enzyme inhibitory, and immunosuppressive effects, underscoring the genus's significant research value and potential applications (Chen et al., 2024).

It is widely recognized that many microbial gene clusters remain silent under standard fermentation conditions. These “silent” or “cryptic” biosynthetic gene clusters may encode novel natural products, representing a vast reservoir of potential drug candidates. The “one strain many compounds” (OSMAC) approach, pioneered by Professor Zeeck and colleagues, involves altering medium composition and other parameters to activate these silent genes, thereby inducing the production of novel secondary metabolites (SMs) (Bode et al., 2002; Pan et al., 2019). This strategy has proven highly effective in unlocking the biosynthesis of cryptic natural products, yielding novel compounds with significant potential (Pfütze et al., 2024; Zhang et al., 2015).

Xylaria longipes HFG1018, isolated from the medicinal fungus *Fomitopsis betulina* (Bull.) (Fomitopsidaceae), is a typical ectomycorrhizal fungus within the Xylariaceae family. Fungicolous fungi (FF), having co-evolved with their hosts through long-term natural selection, provide valuable insights into host-fungus interactions through the study of their SMs (Sun et al., 2019). Previous research on *X. longipes* HFG1018 led to the isolation of a series of nor-pimarane diterpenes and two novel bicyclo (2.2.2) octane diterpene skeletons with immunosuppressive properties from its liquid fermentation (Chen et al., 2020). To further explore its chemical diversity, three distinct fermentation systems were employed in this study, resulting in the isolation of 14 new compounds, including three pimarane-type diterpenes (**1**–**3**), one pentapeptide (**4**), nine 6-ethyl 4*H*-chromen-4-one derivatives (diplosporins) (**5**–**13**), and one isochromone

(**14**), alongside 27 known compounds (Figs. 1 and 2). Notably, all new SMs were obtained from rice fermentation. Among these, compound **1** represents the first example of a 6/6/6/6-fused tetracyclic pimarane; compound **4** is a rare pentapeptide; and compound **9** is a novel nordiplosporin.

Psoriasis is an almost incurable skin disease with excessive immune response and over-proliferation of keratinocytes. Antiproliferative assays against induced-T/B lymphocytes (immune cells) and a keratinocyte cell line (HaCaT) revealed that several compounds are promising for anti-psoriasis activity. This study details the isolation, structural elucidation, and bioactivity evaluation of these metabolites, contributing to the growing knowledge on *Xylaria* species and their potential applications.

Methods and materials

General experimental procedures

Optical UV spectra were recorded on a Shimadzu UV-2401PC UV-visible recording spectrophotometer (Shimadzu, Kyoto, Japan). IR spectra (in MeOH) were measured on a Bruker Tensor 27 spectrometer (Bruker, Karlsruhe, Germany). Rotations were calculated using the APIV (Rudolph Research Analytical). All the NMR spectra were obtained on a Bruker Avance III 500 MHz spectrometer (Bruker Corporation, Karlsruhe, Germany). High-resolution electrospray ionization mass spectra (HRESIMS) were recorded using an AB Sciex Triple-TOF 6600 (AB SCIEX, Framingham, MA, USA). Macroporous adsorption resin (Cangzhou Bon Adsorber Technology Co., Ltd, Cangzhou, China), Sephadex LH-20 (Amersham Biosciences, Uppsala, Sweden), and silica gel (Qingdao Haiyang Chemical Co., Ltd, China) were used for column chromatography (CC). Medium-pressure liquid chromatography (MPLC) was performed on the FL-H050G MPLC system (Agela Technologies, Tianjin, China) with an Agela ODS flash column (C-18, 120 g, 40–60 mm, Tianjin, China) or MCI gel (CHP20/P120, Mitsubishi Chemical Corporation, Yokohama, Japan). Preparative high-performance liquid chromatography (prep. HPLC) was performed on a SEP LC-52 equipped with a YMC-pack ODS-A column (dimensions 250 × i.d. 10 mm, particle size 5 μm, 4 mL/min; dimensions 250 × i.d. 20 mm, particle size 5 μm, 7 mL/min; YMC, Tokyo, Japan), and a MWD UV detector (Separation Technology Co Ltd., Beijing, China). All solvents used were of analytical or Chromatographic grades (TJshield Fine Chemicals Co., Ltd, Tianjin, China). All elution systems were described in terms of volume ratio. Concanavalin A (ConA), lipopolysaccharide (LPS, Escherichia coli 055: B5), CCK-8, and RPMI 1640/DMEM media were purchased from Solarbio Life Sciences (Beijing, China). Fetal bovine serum (FBS)

was purchased from HyClone Laboratories (Utah, USA). All elution systems were described in terms of volume ratio.

Fungal material and taxonomy

Sample collection and morphological characterization

The fungus *Xylaria longipes* HFG1018 (Xylariaceae) was isolated from the wood-rotting fungus *Fomitopsis betulina* (Bull.) (Fomitopsidaceae). *F. betulina* was harvested from Changbai Mountain National Nature Reserve, Jilin Province, China, in 2012 and identified by the ITS gene (GenBank accession No. PQ844712). The fungus *Xylaria longipes* was confirmed by combing analysis of the ITS gene (GenBank accession No. PV523290), *TUB2* gene (GenBank accession No. MN583256), and *rpb2* gene (GenBank accession No. PV558833). The sample was preserved in the Department of Traditional Chinese Medicine and Natural Medicinal Chemistry, Henan University of Traditional Chinese Medicine (No. HFG1018).

Pure cultures were maintained at 25 ℃ for 1-4 weeks on oatmeal agar (OA) medium. The mycelium, stained with methylene blue, is examined for microscopic features under a biological microscope. Micro characteristics were observed under an ML11-II biomicroscope (Guangzhou Mingmei Optoelectronic Technology Co., Ltd, China) and photographed by an iPhone 13 Pro camera.

Sequence alignments and phylogenetic analyses

All the obtained sequences were deposited in GenBank (Table S1, Supplementary Information). The obtained sequences were analyzed using the BLAST tool in NCBI GenBank to search for highly similar sequences. Single sequences (ITS, *TUB2*, and *rpb2*) were aligned with the Clustal W algorithm in the MEGA v.12 program and manually adjusted for maximum sequence similarity. Multiple sequences were concatenated using PhyloSuite software (Zhang et al. 2020). Phylogenetic trees were constructed using concatenated sequences (ITS, *TUB2*, and *rpb2*) in MEGA v.12 with the neighbor-joining (NJ) and maximum-likelihood (ML) methods. The multi-locus phylogenetic tree included the fungal isolate studied here and other closely related species of the *Xylaria* genus, with *Engleromyces sinensis* and *Collodiscula bambusae* serving as an outgroup. Clade stability was evaluated with 1 000 bootstrap replicates.

Fermentation, extraction, and isolation

Rice fermentation

Rice fermentation was conducted following established protocols. The glucose peptone yeast (GPY) medium

used for fermenting *X. longipes* contained glucose (5%), peptone from porcine meat (0.15%), yeast powder (0.5%), KH_2PO4 (0.05%), and $MgSO_4$ (0.05%). Two bottles of GPY liquid fermentation medium (350 mL/bottle) inoculated with *X. longipes* were incubated in a shaker at 24°C and 150 rpm for 7 days in the dark. Separately, rice and distilled water (H_2O) were mixed at a mass ratio of 1:1.3 (total rice weight: 20 kg) and distributed into 500 mL flasks, which were then autoclaved. The cultured liquid mycelium was subsequently transferred into the sterilized flasks and incubated in the dark for 40 days.

After fermentation, the rice substrate was transferred to an extraction tank and subjected to ultrasound-assisted extraction with 95% ethanol for 3 hours per cycle. This process was repeated three times. The ethanol solution containing metabolites was concentrated under reduced pressure until only water remained. The aqueous concentrate was then extracted four times with an equal volume of ethyl acetate (EtOAc). The EtOAc layer was concentrated under reduced pressure to yield 233.9 g of crude extract. This crude extract was further fractionated using macroporous adsorption resin column chromatography (CC) with a gradient of EtOH–H2O (20:80, 40:60, 60:40, 80:20, 100:0), resulting in nine fractions (A–I).

Fractions B–D (68.3, 14.8, and 4.2 g, respectively) and fraction F (27.9 g) were further separated using medium-pressure liquid chromatography (MPLC). Fractions B–D were processed on an MCI gel column, while fraction F was separated on a C18-ODS column, both employing a gradient elution of methanol (MeOH) in H_2O (20:80, 40:60, 60:40, 80:20, 100:0). This yielded four to six subfractions for each fraction (B1–B4, C1–C5, D1–D7, and F1–F6, respectively).

Subfraction B2 was subjected to Sephadex LH-20 column chromatography using MeOH as the eluent, resulting in six parts (B2a–B2f). Compounds **5** (286.8 mg, t_R = 20.7 min) and **6** (57.0 mg, t_R = 20.0 min) were purified from fraction B2d using preparative HPLC with a gradient of acetonitrile (MeCN)/H_2O (15:85→100:0, 50 min, 4 mL/min).

Subfraction C1 was fractionated into three parts (C1a–C1c) via Sephadex LH-20 (MeOH). Fraction C1a was further separated using Sephadex LH-20 (acetone), yielding four subfractions (C1a1–C1a4). Fraction C1a1 was separated by prep. HPLC (MeCN/H_2O 35:65→80:20→100:0, 0→50→60 min, 4 mL/min) to give compounds **23** (16.5 mg, t_R = 14.7 min) and **25** (347.9 mg, t_R = 13.0 min). Fraction C1a2 was eluted on a silica gel CC with an isocratic elution of petroleum ether–acetone (1:1) to afford four components (C1a2a–C1a2d). Compounds **7** (61.1 mg, t_R = 17.3 min) and **11** (5.1 mg, t_R = 28.2 min) were purified from fraction

C1a2a using prep. HPLC (MeCN/H_2O 20:80→70:30, 60 min, 4 mL/min). Compounds **22** (2.9 mg, t_R = 30.8 min) and **14** (1.5 mg, t_R = 31.9 min) were isolated from fraction C1a2c via prep. HPLC with an isocratic elution of MeCN/H_2O (30:70, 4 mL/min). Fraction C1a2d was separated via prep. HPLC (MeOH/H_2O 50:50→100:0, 30 min, 8 mL/min), yielding three components (C1a2d1–C1a2d3). Compounds **26** (7.4 mg, t_R = 16.5 min), **9** (6.7 mg, t_R = 36.9 min), and **12** (17.4 mg, t_R = 41.1 min) were obtained from fraction C1a2d1.

Fraction C2 was separated on silica gel CC with an isocratic elution of petroleum ether–acetone (1:1), yielding two components (C2a and C2b). Compounds **10** (58.6 mg, t_R = 28.8 min), **7** (7.3 mg, t_R = 29.7 min), and **24** (43.6 mg, t_R = 39.2 min) were purified from fraction C2a using prep. HPLC (MeCN/H_2O 25:75→100:0, 50 min, 4 mL/min).

Fraction D5 was separated using MPLC equipped with a C18-ODS column, employing a gradient elution of MeOH in H_2O (20:80, 40:60, 60:40, 80:20, 100:0), resulting in six subfractions (D5a–D5f). Fraction D5b was further purified using Sephadex LH-20 (MeOH), yielding three components (D5b1–D5b3). Compound **19** (4.7 mg, t_R = 23.8 min) was obtained from fraction D5b3 via prep. HPLC (MeCN/H_2O 30:70→100:0, 50 min, 4 mL/min).

Fractions F1 to F4 were subjected to Sephadex LH-20 (MeOH) chromatography, yielding three or four components each (F1a–F1c, F2a–F2c, F3a–F3c, and F4a–F4d). Compound **20** (30.2 mg, t_R = 28.5 min) was isolated from fraction F1b using prep. HPLC (MeCN/H_2O 15:85→40:60, 70 min, 3 mL/min). Compounds **21** (34.3 mg, t_R = 35.0 min) and **28** (2.4 mg, t_R = 37.6 min) were obtained from fraction F2c via prep. HPLC with an isocratic elution of MeCN/H_2O (30:70, 3 mL/min). Compound **27** (3.4 mg, t_R = 24.7 min) was obtained from fraction F3c using prep. HPLC (isocratic elution of MeOH/H_2O 71:29, 7 mL/min). Compound **3** (4.9 mg, t_R = 35.1 min) was isolated from fraction F4b via prep. HPLC (MeCN/H_2O 20:80→60:40, 55 min, 4 mL/min).

Fraction F5 was separated using MPLC equipped with an MCI gel column by a gradient eluent of MeOH in H_2O (20:80, 40:60, 60:40, 80:20, 100:0), yielding seven subfractions (F5a–F5g). Fractions F5d, F5f, and F5g were dealt with Sephadex LH-20 (MeOH), resulting in three or five components each (F5d1–F5d3, F5f1–F5f5, and F5g1–F5g5). Compounds **16** (141.8 mg, t_R = 10.6 min), **17** (72.2 mg, t_R = 43.9 min), and **2** (16.6 mg, t_R = 44.6 min) from fraction F5d2 via prep. HPLC (isocratic elution of MeCN/H_2O 42:58, 4 mL/min). Compound **4** (7.44 mg, t_R = 24.5 min) was obtained from fraction F5f1 using prep. HPLC

(MeCN/H2O 38:62 → 70:30, 40 min, 4 mL/min). Compound **15** (8.7 mg, t_R = 16.5 min) was purified from fraction F5f4 using prep. HPLC (MeCN/H_2O 62:38, 4 mL/min). Compound **18** (41.5 mg, t_R = 9.8 min) was isolated from fraction F5g2 using prep. HPLC (MeCN/H_2O 60:40→100:0, 20 min, 4 mL/min). Compound **29** (2.3 mg, t_R = 12.5 min) from fraction F5g3 using prep. HPLC (MeCN/H_2O 60:40→100:0, 20 min, 4 mL/min). Finally, compound **1** (1.3 mg, t_R = 17.5 min) was purified from fraction F5g5 using prep. HPLC (60:40→100:0, 20 min, 4 mL/min).

Liquid fermentation of potato dextrose broth (PDB)

The culture medium for fermenting *X. longipes* was prepared using potato (200 g), peptone from porcine meat (1.0 g), dextrose (20.0 g), KH_2PO4 (3.0 g), and $MgSO_4$ (1.5 g) dissolved in deionized H_2O (1.0 L). A total of 20 L of the culture medium was inoculated with the *X. longipes* strain and incubated at 24 °C with shaking at 150 rpm on rotary shakers for 28 days in a dark environment. After 7 days of fermentation, 3-methyl-2-butenol was added to the broth at a 400 mg/L concentration.

Following fermentation, the 20.0 L broth was separated into supernatant and mycelia by centrifugation. The supernatant was concentrated under reduced pressure, and the resulting residue was partitioned between ethyl acetate (EtOAc) and H_2O. Simultaneously, the mycelia were extracted three times with ethanol (EtOH). The EtOH extract was evaporated and similarly partitioned between EtOAc and H_2O four times. The combined EtOAc layers yielded a total weight of 24 g.

The EtOAc extract underwent MPLC using a C18-ODS column, eluted by a gradient eluent of MeOH in H_2O (20:80, 40:60, 60:40, 80:20, 100:0), yielding five fractions (A–E). Fractions B (5.6 g) and D (9.7 g) were separated over silica gel CC eluted with petroleum ether–acetone (2:1, 1:1, 0:1), giving 12 (B1–B12) and eight fractions (D1–D8). Compound **30** (178.6 mg, t_R = 27.9 min) was purified from fraction B2 via prep. HPLC (MeCN/H_2O 34:66→69:31→100:0, 0→35→45 min, 4 mL/min).

Subfraction D4 was further purified by preparative prep. HPLC using a gradient eluent (MeCN/H2O 80:20→100:0, 15 min, 4 mL/min) to afford compounds **31** (4.1 mg, t_R = 27.9 min) and **33** (1.3 mg, t_R = 40.5 min). Fraction D2 was subjected to prep. HPLC (MeCN/H_2O 51:49→95:5, 35 min, 4 mL/min) gives 12 components (D2a–D2l). Compounds **34** (1.2 mg, t_R = 38.4 min) from fraction D2e (MeCN/H_2O 60:40→100:0, 45 min, 4 mL/min) and **32** (4.0 mg, t_R = 43.5 min) from fraction D2h (MeCN/H_2O 80:20→100:0, 45 min, 4 mL/min) via prep. HPLC.

Liquid fermentation of glucose peptone yeast (GPY)

45.0 L of the GPY culture medium was inoculated with *X. longipes* strain and was then incubated at 24 °C and 150 rpm on rotary shakers for 28 days in a dark environment. After fermentation for 7 days, 3-methyl-2-butenol was added (400 mg/ L).

After a procedure similar to PDB fermentation, 45.0 L GPY fermentation, and mycelium gave an EtOAc layer (41.5 g). The EtOAc extract underwent macroporous adsorption resin CC eluted with an EtOH/H_2O gradient (20:80, 40:60, 60:40, 80:20, 100:0), yielding four fractions (A–D). Fraction C (3.4 g) was separated on MPLC (C18-ODS column) and eluted with a MeOH/H_2O gradient (20:80, 40:60, 60:40, 80:20, 100:0), yielding eight fractions (C1–C8). Fractions C3 (MeOH/H_2O, 20:80→100:0, 30 min, 7 mL/min) and C6 (MeOH/H_2O 50:50→100:0, 45.0 min, 7 mL/min) were further separated over prep. HPLC to provide eight (C3a–C3h) or three fractions (C6a–C6c), respectively. Compounds **37** (2.6 mg, t_R = 8.7 min) from fraction C3d (MeCN/H_2O 22:78, 4 mL/min), **39** (4.6 mg, t_R = 14.5 min) from fraction C3h (MeCN/H_2O 20:80→50:50, 30 min, 4 mL/min), **38** (2.4 mg, t_R = 10.4 min) from fraction C6b (MeCN/H_2O 35:65→65:35→100:0, 0→35→50 min, 3 mL/min), and **41** (5.5 mg, t_R = 28.9 min) from fraction C6c (MeCN/H_2O 35:65→65:35→100:0, 0→35→50 min, 4 mL/min) were purified by prep. HPLC. Fraction C5 was separated on MPLC (MCI gel column) eluted with a MeOH/H_2O gradient (20:80, 40:60, 60:40, 80:20, 100:0), yielding six fractions (C5a–C5f). Compounds **36** (9.7 mg, t_R = 8.7 min) from fraction C5c (MeCN/H_2O15:85→70:30→100:0, 0→30→60 min, 4 mL/min), **40** (4.4 mg, t_R = 35.3 min) from fraction C5e (MeCN/H_2O 35:65→60:40→100:0, 0→60→80 min, 4 mL/min), and **28** (2.4 mg, t_R = 38.2 min)/**35** (2.4 mg, t_R = 51.2 min) from fraction C5g (MeCN/H_2O 28:72→28:72→100:0, 0→60→70 min, 4 mL/min) were obtained via prep. HPLC. Fraction D (2.6 g) was subjected to silica gel CC, using a petroleum ether–acetone elution system (2:1, 1:1, 0:1), giving six fractions (D1–D6), and then subfraction D1 was dealt with prep. HPLC (MeCN/H_2O 40:60→75:25→100:0, 0→30→45 min, 4 mL/min) to give compound **25** (4.5 mg, t_R = 23.5 min)

Calculations of ^{13}C NMR and ECD

Conformational analysis of the candidate structures (compounds **1**, **5**, **6**, **13**, and **14**) was performed using the MMFF94s force field. The conformers with a distribution greater than 1% were further optimized at the B3LYP/6-31G(d,p) level of theory in the Gaussian 16 software package. The optimized conformers within

3 kcal·mol^{-1} of the global minimum were selected for additional ^{13}C NMR (**1**, **13**) and ECD (**1**, **5**, **6**, **13**, and **14**) calculations (Supplementary Information).

^{13}C NMR calculation. Gauge-independent atomic orbital (GIAO) calculations of the shielding values of candidates were accomplished by the time-dependent density functional theory (TDDFT) at the mPW1PW91/6-31G(d,p) level in $CHCl_3$ with the IEFPCM model in the Gaussian 16 software package (Frisch et al. 2016). The calculated NMR data of these conformers were averaged according to the Boltzmann distribution theory and their relative Gibbs free energies. The correlation coefficient (R^2) and mean absolute error (MAE) were calculated to evaluate the deviations between the experimental and calculated results. The calculation results were processed by an in-house Excel-based program.

ECD calculation. The theoretical calculations of ECD were performed using TDDFT at B3LYP/6-31G(d,p) level in MeOH with the CPCM model in the Gaussian'16 software package. The calculated ECD curve was generated using SpecDis 1.70.1. The ECD curve of the enantiomers was generated by the function "enantiomeric ECD" in SpecDis (Bruhn et al. 2012).

Bioassays

Assays of immunosuppressive activity, lymphocyte viability, and antiproliferative activity against HaCaT cells

As previously reported, the immunosuppressive activities, lymphocyte viability, and antiproliferative activity against HaCaT cells were evaluated using the CCK-8 method (Zhao et al. 2023, 2024).

In the immunosuppressive and lymphocyte viability, the primary tested concentration of all compounds was 20.0 μM, and dexamethasone (Dex) (c = 2.0 μM) was used as a positive control. In the antiproliferative activity against HaCaT cells, the primary tested concentration of all compounds was 40 μM, and the positive control was methotrexate (MTX) (c = 40.0 μM). When the inhibition rates are greater than 50%, the IC_{50} values of active compounds will be further tested and calculated. All experiments were performed in triplicate.

Cytokine analysis by ELISA of induced T cells

The mononuclear cell suspensions (2×10^5 cells/well) were cultured with ConA (5 μg/mL) in 96-well plates, and indicated concentrations of compounds **2**, **15**, and **32** were added simultaneously. After a 48-hour culture period, cytokines in the supernatants were quantified using mouse IFN-γ, IL-2, and IL-17A ELISA kits

(Mabtech, Sweden), following the manufacturer's protocol (Jing et al. 2021; Zhao et al. 2024).

EdU proliferation assay

EdU fluorescence labeling for cell proliferation of induced T/B lymphocytes (2×10^5 cells/well) and HaCaT cells (1×10^4 cells/well) of active compounds **10**, **19**, **23**, **32**, **38**, and **41** (final concentration 10 or 20 μM) was performed as previously reported (Biram and Shulman 2020; Zhao et al. 2024). EdU (HF488) (the Click-iT™ EdU Flow Cytometry Assay Kit, APExBIO, USA) was added 24 h (final concentration 50 μM, T and B cells) and 4 h (final concentration 10 μM, HaCaT cells) before harvesting the cells. All procedures were performed according to the manufacturer's instructions for the click reaction. EdU-positive cells and proliferating phase cells were analyzed with a fluorescence microscope.

Immunofluorescence protocol (cell climbing slides)

The immunofluorescence protocol was performed using the reported method (Zhao et al. 2024). HaCaT cells (2.0×10^5 cells/well) were plated onto 6-well plates with glass coverslips and adhered overnight (12 h) before compound addition. After treatment with active compounds **10** (final concentration 31 μM) and **32** (final concentration 27 μM) for 36 h, the supernatant was removed, and the cells were washed twice with PBS, fixed with 4% paraformaldehyde for 15 min, and then washed with PBS three times. After blocking, incubated with NF-κB p65 (p65)/phosphorylated NF-κB p65 (p-p65) antibodies, secondary antibodies (Servicebio, China). Then, cells were counterstained with 4,6-diamino-2-phenylindole (DAPI) for 5 min. After the PBS washing, fluorescent seal liquid was added, and the plate was monitored under an imaging system (Pannoramic MIDI, 3Dhistech, Hungary). The nucleus is blue, and positive cells are green (p-p65) or red (p65). The immunofluorescence areas for each indicator were analyzed in Image J.

Statistics and reproducibility

GraphPad Prism 8.0 software was used for statistical data analysis, which was expressed as $\bar{X} \pm s$. One-way ANOVA was used to compare the differences between groups. $P<0.05$ or $P<0.01$ was considered statistically significant.

Ethic Statement

The animal study (No. DWLL202003116) was reviewed and approved by the Animal Welfare Ethics Committee of the Henan University of Chinese Medicine.

Spectroscopic data of compounds

^{1}H, ^{13}C, 2D NMR, HRMS spectra, and computational details of compounds **1**–**14** were listed in the Supplementary material.

11*α*,16-Epoxy-isopimar-8(9)-en-19*β*-oic acid (**1**)

White powders, $[\alpha]_D^{23}$ + 12.2 (*c* 0.01, MeOH); UV (MeOH) λ_{max} (log ε): 201 (4.41), 214 (4.09) nm; IR (MeOH) ν_{max} cm^{-1}: 3338, 2945, 1690, 2833, 1449, 1114,1027; ^{1}H NMR (500 MHz $CDCl_3$) data see Table 1; ^{13}C NMR (125 MHz $CDCl_3$) data see Table 1; HR-ESI-MS *m/z* 319.2269 $[M + H]^+$ (calcd for $C_{26}H_{31}O_3$, 319.2268).

16-*α*-*D*-Mannopyranosyloxyisopimar-8(9)-en-19-oic acid (**2**)

Colorless oils, $[\alpha]_D^{23}$ + 27.2 (*c* 0.06, MeOH), UV (MeOH) λ_{max} nm (log ε): 201 (3.91), 241 (3.58); IR (MeOH) ν_{max} cm^{-1}: 3374, 2934, 1697, 1645, 1024; ^{1}H NMR (500 MHz DMSO-d_6) data see Table 2; ^{13}C NMR (125 MHz DMSO-d_6) data see Table 2; HR-ESI-MS *m/z* 505.2773 $[M + Na]^+$ (calcd for $C_{26}H_{42}O_8Na$, 505.2772).

16-*α*-*D*-Glucopyranosyloxyisopimar-8(9)-en-19-oic acid (**3**)

White powders, $[\alpha]_D^{23}$ + 88.9 (*c* 0.05, MeOH), UV (MeOH) λ_{max} nm (log ε): 201 (3.88), 242 (3.55); IR (MeOH) ν_{max} cm^{-1}: 3288, 2933, 1696, 1457, 1034; ^{1}H NMR (500 MHz DMSO-*d*6) data see Table 2; ^{13}C NMR (125 MHz DMSO-d_6) data see Table 2; HR-ESI-MS *m/z* 505.2770 $[M + Na]^+$ (calcd for $C_{26}H_{42}O_8Na$, 505.2772)

Cyclo(*L*-Phe-*L*-Val-*D*-Ile-*L*-Leu-*L*-Pro) (**4**)

White powders, $[\alpha]_D^{23}$ −64.4 (*c* 0.03, MeOH), UV (MeOH) λ_{max} nm (log ε): 209 (3.72), 244 (3.12), 307 (2.90); IR (MeOH) ν_{max} cm^{-1}: 3275, 2960, 1634, 1541, 1445; ^{1}H NMR (500 MHz DMSO-d_6) data see Table 3; ^{13}C NMR (125 MHz DMSO-d_6) data see Table 3; HR-ESI-MS *m/z*: 568.3499 $[M-H]^-$ (calcd for $C_{31}H_{46}O_5N_5$, 568.3504).

Diplosporin A (**5**)

Yellow oils, $[\alpha]_D^{23}$ + 47.9 (*c* 0.15, MeOH), UV (MeOH) λ_{max} nm (log ε): 211 (5.58), 251 (5.59); IR (MeOH) ν_{max} cm^{-1}: 3396, 2937, 1660, 1611, 1456, 1106, 1032; ^{1}H NMR (500 MHz $CDCl_3$) data see Table 4; ^{13}C NMR (125 MHz $CDCl_3$) data see Table 5; HR-ESI-MS *m/z* 261.1097 $[M + Na]^+$ (calcd for $C_{13}H_{18}O_4Na$, 261.1103).

Diplosporin B (**6**)

White powders, $[\alpha]_D^{23}$ + 41.3 (*c* 1.21, MeOH), UV (MeOH) λ_{max} nm (log ε): 213 (3.90), 254 (3.91); IR (MeOH) ν_{max} cm^{-1}: 3418, 2947, 1658, 1592, 1457, 1108, 1030; ^1H NMR (500 MHz $CDCl_3$) data see Table 4; ^{13}C NMR (125 MHz $CDCl_3$) data see Table 5; HR-ESI-MS *m/z* 261.1093 $[M + Na]^+$ (calcd for $C_{13}H_{18}O_4Na$, 261.1103).

Diplosporin C (**7**)

Yellow powders, $[\alpha]_D^{23}$ + 11.8 (*c* 0.37, MeOH), UV (MeOH) λ_{max} nm (log ε): 222 (3.76), 245 (3.77); IR (MeOH) ν_{max} cm^{-1}: 2934, 2876, 2828, 1660, 1620, 1435, 1088; ^1H NMR (500 MHz $CDCl_3$) data see Table 4; ^{13}C NMR (125 MHz $CDCl_3$) data see Table 5; HR-ESI-MS *m/z* 275.1253 $[M + Na]^+$ (calcd for $C_{14}H_{20}O_4Na$, 275.1259).

Diplosporin D (**8**)

Yellow oils, $[\alpha]_D^{23}$ − 25.6 (*c* 0.10, MeOH), UV (MeOH) λ_{max} nm (log ε): 212 (3.75), 253 (3.74); IR (MeOH) ν_{max} cm^{-1}: 2928, 1662, 1622, 1435, 1308, 1197, 1086, 949; ^1H NMR (500 MHz $CDCl_3$) data see Table 4; ^{13}C NMR (125 MHz $CDCl_3$) data see Table 5; HR-ESI-MS *m/z* 253.1435 $[M + H]^+$ (calcd for $C_{14}H_{21}O_4$, 253.1440).

Diplosporin E (**9**)

Yellow powders, $[\alpha]_D^{23}$ + 40.7 (*c* 0.04, MeOH), UV (MeOH) λ_{max} nm (log ε): 210 (3.63), 251 (3.70); IR (MeOH) ν_{max} cm^{-1}: 3364, 2960, 1650, 1600, 1438, 1144, 1020; ^1H NMR (500 MHz $CDCl_3$) data see Table 4; ^{13}C NMR (125 MHz $CDCl_3$) data see Table 5; HR-ESI-MS *m/z* 217.0838 $[M + Na]^+$ (calcd for $C_{11}H_{14}O_3Na$, 217.0841).

Diplosporin F (**10**)

Yellow oils, UV (MeOH) λ_{max} nm (log ε): 229 (3.86), 282 (3.73); IR (MeOH) ν_{max} cm^{-1}: 1659, 1636, 1605, 1451, 1202, 1114; ^1H NMR (500 MHz $CDCl_3$) data see Table 6; ^{13}C NMR (125 MHz $CDCl_3$) data see Table 5; HR-ESI-MS *m/z* 243.0988 $[M + Na]^+$ (calcd for $C_{13}H_{16}O_3Na$, 243.0997).

Diplosporin G (**11**)

Yellow powders, UV (MeOH) λ_{max} nm (log ε): 205 (3.57), 227 (3.70), 251 (3.35), 310 (3.09); IR (MeOH) ν_{max} cm^{-1}: 2966, 2932, 1647, 1615, 1483, 11452, 1313, 1099, 828; ^1H NMR (500 MHz $CDCl_3$) data see Table 6; ^{13}C NMR (125 MHz $CDCl_3$) data see Table 5; HR-ESI-MS *m/z* 219.1018 $[M + H]^+$ (calcd for $C_{13}H_{15}O_3$, 219.1021).

Diplosporin H (**12**)

Yellow powders, $[\alpha]_D^{23}$ + 74.1 (*c* 0.16, MeOH), UV (MeOH) λ_{max} nm (log ε): 223 (3.69), 242 (3.70); IR (MeOH) ν_{max} cm^{-1}: 1708, 1647, 1598, 1476, 1243, 1084, 1025; ^1H NMR (500 MHz $CDCl_3$) data see Table 6; ^{13}C NMR (125 MHz CDCl3) data see Table 5; HR-ESI-MS *m/z* 259.0940 $[M + Na]^+$ (calcd for $C_{13}H_{16}O_4Na$, 259.0941).

Diplosporin I (**13**)

Yellow oils, $[\alpha]_D^{23}$ − 35.4 (*c* 0.01, MeOH), UV (MeOH) λ_{max} nm (log ε): 213 (3.74), 253 (3.74); IR (MeOH) ν_{max} cm^{-1}: 3377, 1653, 1582, 1033, 991; ^1H NMR (500 MHz $CDCl_3$) data see Table 6; ^{13}C NMR (125 MHz $CDCl_3$) data see Table 5; HR-ESI-MS *m/z* 255.1223 $[M + H]^+$ (calcd for $C_{13}H_{19}O_5$, 255.1227).

(*R*)-8-methoxy-3-(methoxymethyl)isochroman-1-one (**14**)

White powders, $[\alpha]_D^{23}$ + 96.2 (*c* 0.02, MeOH), UV (MeOH) λ_{max} nm (log ε): 209 (3.72), 244 (3.12), 307 (2.90); IR (MeOH) ν_{max} cm^{-1}: 1708, 1647, 1598, 1476, 1243, 1084, 1025; ^1H NMR (500 MHz $CDCl_3$) data see Table 7; ^{13}C NMR (125 MHz CDCl3) data see Table 7; HR-ESI-MS *m/z* 223.0974 $[M + H]^+$ (calcd for $C_{12}H_{15}O_4$, 223.0965).

Results and Discussion

Identification of the strain

The strain of *Xylaria longipes* HFG1018 was identified by employing both genetic analysis and morphological characterization. Colonies *Xylaria longipes* HFG1018 grown on OA at 25 °C for 4 weeks, with a diameter of 5 cm, white, velvety or inflorescence, appressed with entire margins; reverse white. No conidia were observed (Fig. 3). For molecular identification, each gene sequence was analyzed using the BLAST algorithm in NCBI, and the results showed that these sequences had the highest homology to the corresponding gene sequences of *Xylaria longipes*. All the gene sequences were deposited in the GenBank database, and the corresponding accession numbers were PV523290 (ITS), MN583256 (*TUB2*), and PV558833 (*rpb2*). The ML and NJ phylogenetic trees constructed using MEGA v. 12 software indicated that isolate HFG1018 clustered with the reference strain *X. longipes* CBS 148.73 (Franco et al., 2021) (Fig. 4). Therefore, the isolate HFG1018 in this study was confirmed as *X. longipes* through phylogenetic analysis.

Structure elucidation of previously undescribed fungal metabolites (*1–14*)

The study identified 41 secondary metabolites from the ethyl acetate (EtOAc) layers of three fermentations

of *X. longipes*. Among these, compounds **1**–**14** were found to be previously undescribed derivatives (Figs. 1 and 2).

Compound **1** was isolated as a white powder, and its molecular formula was determined to be $C_{26}H_{30}O_3$ based on HRESIMS data, showing an ion at *m/z* 319.2269 $[M + H]^+$ (calculated for $C_{26}H_{31}O_3$, 319.2268), indicating 12 degrees of unsaturation. The ^{1}H NMR spectrum exhibited signals for three methyl singlets (δ_H 0.85, 0.92, 1.27) and three protons attached to oxygenated carbons (δ_H 4.30, 3.61, 3.53) (Table 1). The ^{13}C NMR spectrum revealed 20 carbon signals, including three methyls (δ_C 18.2, 28.7, 31.8), eight sp^3 methylenes (δ_C 19.3, 20.5, 32.0, 36.0, 37.8, 40.1, 40.9, 44.3), one sp^3 oxygenated methylene (δ_C 58.5), one sp^3 methine (δ_C 53.3), one sp^3 oxygenated methine (δ_C 66.9), three sp^3 quaternary carbons (δ_C 27.6, 38.2, 43.7), a tetrasubstituted double bond (δ_C 133.3, 134.7), and one carbonyl (δ_C 181.2) (Table 1). The NMR data of **1** closely resemble those of the co-isolated 16-hydroxyisopimar-7-en-19-oic acid (**15**) (Wu et al. 2011), suggesting that **1** is an isopimarane-type diterpenoid (Fig. 1). The presence of a carboxyl group (COOH-19) and a hydroxymethyl group (CH_2O-16) was confirmed by HMBC correlations (CH_3-18 to C-19) and ^{1}H-^{1}H COSY correlations (H_2-15 to H_2-16), consistent with the isopimarane family from *Xylaria* species (Shiono et al. 2009; Wang et al. 2021; Zhou et al. 2021). HMBC correlations (H_3-20 to C-9) and ^{1}H-^{1}H COSY correlations (H_2-11 to H_2-12) indicated an additional hydroxy group at C-11 and a double bond at C-8(9) (Fig. 5). While three rings, one carboxyl, and one double bond accounted for five degrees of unsaturation, the remaining degree required an additional ring. Due to the absence of key HMBC correlations from H_2-16 or H-11 to other carbons, the ring formation was deduced indirectly. Among the possible positions (OH-16, OH-11, and COOH-19), COOH-19 was ruled out because of its distance from both OH-16 and OH-11, as well as its typical chemical shift (δ_C 181.2) for a carboxyl group (Chen et al. 2020; Shiono et al. 2009; Zhou et al. 2021). Thus, it was proposed that the ring form between OH-11 and OH-16. This was supported by a comparison with xylarinorditerpene I, an 18-nor-isopimarane containing a cyclohexyl ether between C-11 and C-13, previously isolated from the same fungus (Chen et al. 2020). The chemical shifts of the oxygenated methine at C-11 [$\delta_{C/H}$ 66.9/4.30 (dd, J = 2.5, 2.5 Hz)] and the oxygenated methylene at C-16 [$\delta_{C/H}$ 58.5/3.61 (ddd, J = 13.1, 11.4, 3.1 Hz); 3.53 (dd, J = 11.4, 5.8 Hz)] in compound **1** matched those of xylarinorditerpene I [$\delta_{C/H}$ 66.4/4.34 (dd, J = 2.5, 2.5 Hz), -CHO-11; $\delta_{C/H}$ 58.6/3.67 (ddd, J = 13.2, 11.6, 2.9 Hz) & 3.54 (dd, J = 11.6, 6.1 Hz), -CH_2O-16], confirming an ether bond between C-11 and C-16 in **1**.

The relative configuration of **1** was determined using ROESY data (Fig. 5). The cross-peaks of H_3-18/H-5 and H_3-18/H-6α (δ_H 2.00) indicated their *α*-orientation. In contrast, cross-peaks of H_3-20/H-11, H_3-20/H-6*β* (δ_H 1.85), H-11/H-12*β* (δ_H 1.71), and H-12*β*/H_3-17 suggested an 11*β*-H and a 17*β*-CH_3. Finally, the absolute configuration and structural validity of compound **1** were confirmed by comparing experimental ECD and ^{13}C NMR data with calculated spectra using Gaussian 09. The calculated results matched the experimental data (Figs. 6A and 6B), assigning **1** as 11*α*,16-epoxy-isopimar-8(9)-en-19*β*-oic acid.

Compound **2** was isolated as colorless oils. Its molecular formula, $C_{26}H_{42}O_8$, matched that of co-isolate **16**, indicating six degrees of unsaturation. The ^{1}H NMR data of **2** (Table 2) and HSQC spectrum exhibited characteristic resonances of three methyl singlets (δ_H 0.85, 0.89, and 1.15). Additionally, the distinctive signal of an anomeric proton at δ_H 4.55 (1H, brs), alongside eight protons ranging from δ_H 3.28 to 3.64, suggested the presence of a hexose unit and an oxygenated methylene group. The ^{13}C NMR (Table 2) and DEPT spectra confirmed the presence of 26 carbons, assigned as three methyl groups, ten methylenes (one oxygenated at δ_C 63.2), one methine, three sp^3 quaternary carbons, two olefinic quaternary carbons (δ_C 124.8 and 135.0), a carbonyl (δ_C 178.9), and six carbons from the glycosyl. Overall, the NMR data of **2** closely resembled those of 16-*α*-D-mannopyranosyloxyisopimar-7-en-19-oic acid (**16**) (Shiono et al. 2009). The only difference between **2** and **16** was the location of the double bond. HMBC correlation from H_3-20 to C-9 indicated that the double bond was located at C-8(9) in 2 instead of C-7(8) in **16**. The ROESY correlations of H_3-18/H-5, H_3-18/H_2-3, H_3-18/H-6*α* (δ_H 1.85), and H3-20/H-6*β* (δ_H 1.72) showed that H_3-18 was *α*-oriented while H_3-20 was *β*-oriented. Moreover, ROESY correlations of H_3-17/H_2-14 (δ_H 1.65, 1.60) and H2-16*β* (δ_H 3.67)/H2-14α (δ_H 1.65) were observed, suggesting that H_3-17 was *β*-oriented (Fig. 5).

According to the literature (Shiono et al. 2009; Wang et al. 2021; Zhou et al. 2021), only two pyranoses consisting of isopimarane from the *Xylaria* species have been identified: *α*-D-mannose and α-D-glucose, which can be assigned easily by comparing NMR analysis. In this work, compounds **2**, **16**, and **17** were obtained simultaneously, with the weights of compound **16**, which has an *α*-D-mannose moiety, and compound **17**, which has an *α*-D-glucose moiety, being larger than that of compound **2**. Their NMR data, measured in DMSO-d6, were carefully analyzed. The ^{13}C NMR data of the pyranoses in compound **2** were nearly identical to those of compound **16**, with the largest deviation (Δ_{max}) being 0.05 ppm (C5') (Supplementary Information, Fig. S90), indicating that the pyranose in compound **2** is *α*-D-mannose.

Additionally, observed ROESY correlations of H-1'/H-2'/H-3'/H-5' and unobserved ROESY correlations of H-2'/H-4' followed the configuration of α-D-mannose. Therefore, the structure of compound **2** was determined as 16-α-D-mannopyranosyloxyisopimar-8(9)-en-19-oic acid.

Compound **3** was isolated as colorless oils. The HRESIMS spectra of compound 3 suggested a molecular formula of $C_{26}H_{42}O_8$, identical to those of compounds **2**, **16**, and **17**. The ^{1}H and ^{13}C NMR data of compound **3** were extremely similar to those of compound **2**, except for the resonances of the glycosyl at C-1'−C-6' (**2**: δ_C 99.8, 70.4, 71.1, 67.0, 74.1, 61.3; **3**: δ_C 98.6, 71.9, 73.3, 70.3, 72.8, 61.0) (Table 2). Further analysis of the 2D NMR data confirmed that compounds **2** and **3** shared the same planar structure but differed in glycosyl (Fig. 5). Considering the similar biosynthetic pathways, J value of H-1' (J = 3.4 Hz), ROESY correlations (H-1'/H-2'/H-4'/H2-6') (Fig. 3), and comparing the chemical shifts of C-1'−C-6' of compound **3** to those of compound **17** [the Δ_{max} is 0.13 ppm (C1')] (Supplementary Information, Fig. S90), this pyranose in compound 3 was deduced to be α-D-glucose. The remaining configurations of compound 3 were determined to be the same as those of compound **2** due to their identical key ROESY correlations (Fig. 5). Thus, the structure of compound 3 is 16-α-D-glucopyranosyloxyisopimar-8(9)-en-19-oic acid.

As illustrated above, compounds **2** and **3** exhibit identical planar structures and nearly identical configurations, with the only difference being the orientation of the 4'-OH group in the glycosyl moiety. Consequently, their circular dichroism (CD) spectra display similar trends as their calculated electronic circular dichroism (ECD) spectra. Only the ECD spectrum of compound **3** was calculated and compared with the experimental spectra of **2** and **3**. As shown in Fig. 6C, the diterpenoid moieties of **2** and **3** were determined to have the absolute configurations 5*R*, 9*S*, 10*R*, and 13*S*.

Compound **4**, isolated as a colorless powder, had a molecular formula of $C_{31}H_{46}O_5N_5$ based on its HRESIMS and comprised 14 mass units (CH_2) less than compound **18** (Wu et al. 2011). Analysis of the ^{1}H, ^{13}C, DEPT and HSQC NMR spectroscopic data of **4** (Table 3) revealed the presence of three amide protons (*N*-H δ_H 7.07, 8.34, 8.35 and 8.42, respectively), six methyl groups (including five methyl singlets, and one methyl triplet), six methylenes (including one *N*-methylene), eight methines (five of which are heteroatom-bonded), one monosubstituted benzene, and five carboxylic carbons. Analysis of the ^{1}H and ^{13}C NMR spectroscopic data of **4** (Table 3) revealed its structural features similar to those of compound **18**, except that N-H replaced the signals for the *N*-Me. These observations were confirmed by relevant ^{1}H-^{1}H COSY and

HMBC correlations (Fig. 7). By using COSY and HSQC, the independent spin systems of the type X-CH(NH)-CH_2-CH_2-CH_2-X', X-CH(NH)-$CH(CH_3)_2$, X-CH(NH)-$CH(CH_3)$-CH_2-CH_3, and X-CH(NH)-CH_2-$CH(CH_3)_2$ were identified, indicating the presence of proline, valine, isoleucine, and leucine residues. The remaining independent spin system of the type X-CH(NH)-CH_2-X', together with the HMBC correlations from βH (Phe) to the γ and ortho carbons of the benzene, and from H-*N* (δ_H 8.42) to CO (Phe), established the phenylalanine (Phe) unit. Because only 10 of the calculated 11 degrees of unsaturation could be accounted for, it became clear that **4** was a cyclic peptide. Upon extensive analysis of these data, compound **4** was assigned as a cyclic pentapeptide containing one equivalent each of valine, leucine, isoleucine, phenylalanine, and proline. The carbonyl carbons within each residue were assigned from HMBC correlations between the C=O and their respective α and *N* protons (Table 3 and Fig. 7), which established the complete amino acid sequence of **4** as cyclo-(-Phe-Pro-Leu-Ile-Val-). Since the NMR data (Table 3), optical rotation (Fig. 7), and experimental CD spectrum (Supplementary Information, Fig. S100) of the **4** ($[\alpha]_D^{23}$ −64.4) were quite similar to those of **18** ($[\alpha]_D^{23}$ − 46.8) (Wu et al. 2011), indicating the *L* configuration for Phe, Val, Ile, Leu, Pro, and D configuration for Ile.

Compound **5** was isolated as a yellow oil. HRMS analysis confirmed its formula as $C_{13}H_{18}O_4$ (indicating five double bond equivalents). Analysis of the ^{1}H NMR spectrum of **5** (Table 4) identified 17 of the 18 protons, including an olefinic hydrogen (δ_H 7.99, brs), three hydrogens on oxygen carbons [δ_H 4.83 (d, J = 2.2 Hz), 4.31 (d, J = 13.7 Hz), 4.27 (d, J = 13.7 Hz)], five multiple protons (δ_H 1.37−2.66), a triplet methyl (δ_H 1.04), and a methoxy group (δ_H 3.40). The ^{13}C NMR spectrum clearly showed all 13 carbon atoms and was supported by the HRMS data. Analysis of the HSQC and ^{13}C NMR data (Table 5) led to the assignment of two pairs of trisubstituted double bonds (δ_C 125.2, 126.0, 155.2, and 168.8), one conjugated methine (δ_C 179.2), four sp^3 methylenes (δ_C 22.7, 25.3, 28.8, and 67.0), two sp^3 methines (δ_C 42.0, 62.3), a methyl (δ_C 11.9), and a methoxy (δ_C 58.9). Since the 1D NMR data of **5**, including carbon types, chemical shifts, and the J values were almost identical to those of (5*R*,6*R*) 6-ethyl-5-hydroxy-3-(methoxymethyl)-5,6,7,8-tetrahydro-4*H*-chromen-4-one (Masahiko et al. 2014), their planar structure and relative configuration were determined to be the same, which was further supported by HMBC (H_3-11 to C-6/C-10, H_3-12 to C-9, H-2 to C-9/C-4a/C-8a, H2-9 to C-3/C-5, H-5 to C-3, and H-6 to C-5) and ROESY correlations (H_2-10/H-5/H-6, and H_3-11/H-5) (Fig. 8). For compound **5**, the doublet of H-5 with a small J value (J = 2.2 Hz) was attributed

to the Jae coupling of H-5/H-6, as observed in Newman projection analysis (Fig. 8). Hence, the relative configuration of 5 is 5*R**,6*R**. To determine the absolute configuration of 5, the ECD trends for two possible configurations, (5*S*,6*S*)-**5** (**5a**) and (5*R*,6*R*)-**5** (**5b**), were calculated in the Gaussian 16 program (Supplementary Information). Based on the comparison of results, the ECD spectrum of **5a** matched the experimental one more closely than that of **5b** (Fig. 9). Finally, the structure of **5** was defined as (5*S*,6*S*) 6-ethyl-5-hydroxy-3-(methoxymethyl)-5,6,7,8-tetrahydro-4H-chromen-4-one and named diplosporin A.

Diplosporin B (**6**) was isolated as a white powder. It shares the same molecular formula ($C_{13}H_{18}O_4$) as that of **5**, based on their HRESIMS spectra. The 1D NMR data of **5** and **6** (Tables 4 and 5) were very similar, except for the resonances of CH-5 [**5**: $\delta_{C/H}$ 62.3/4.83 (d, J = 2.2 Hz); **6**: $\delta_{C/H}$ 69.0/4.59 (d, J = 7.7 Hz)]. Further analysis of the 2D NMR spectra of compound **6** (Fig. 8) indicated that it shared the same planar structure as compound **5**, while the NMR differences suggested an opposite configuration of C-5. Unlike compound **5**, the large coupling constant (J = 7.7 Hz) of H-5 in 6 was attributable to a J_{aa} coupling of H-5/H-6, based on Newman projection analysis (Fig. 8). Meanwhile, the ROESY correlations [H-5/H_2-10, H-5/H-7β (δ_H 1.45), H-6/H-7α (δ_H 2.03)] showed that H-5 and H-6 were located on opposite sides. In other words, the relative configurations of C-5 and C-6 in compound **6** were 5*R** and 6*S**. To identify the absolute configuration of **6**, the ECD spectra for the two possible configurations, (5*R*,6*S*)-**6** (**6a**) and (5*S*,6*R*)-**6** (**6b**), were calculated. As shown in Fig. 9, the ECD spectrum of **6b** was more comparable to the experimental one than that of 6a. Finally, the structure of compound **6** was defined as (5*S*,6*R*) 6-ethyl-5-hydroxy-3-(methoxymethyl)-5,6,7,8-tetrahydro-4H-chromen-4-one.

Diplosporin C (**7**) was isolated as a yellow powder. Its molecular formula is $C_{14}H_{20}O_4$ by HRESIMS analysis, bearing 14 mass units (CH_2) more than **5**. Moreover, the general features of its NMR data (Tables 4 and 5) closely resembled those of compound **5**, indicating that they had analogous structures. Further analysis of the NMR data between compounds **5** and **7** revealed that the main difference was the presence of an additional methoxy ($\delta_{C/H}$ 60.2/3.54) for **7**, which was substituted at C-5 based on the HMBC correlation from H_3-13 to C-5 (Fig. 10). The relative configuration for compound **7** was determined by the JBCA of H-5 and ROESY analysis. The key ROESY correlations of H-6/H-5/H_2-9 and a small coupling constant (J = 1.7 Hz) suggested that the relative configuration was the same as **5**. Finally, the absolute configuration of compound **7** was confirmed as (5*S*,6*S*) by comparing its experimental CD curve with that of compound **5**

(Fig. 9). Therefore, the structure of **7** was defined as (5*S*,6*S*) 6-ethyl-5-methoxy-3-(methoxymethyl)-5,6,7,8-tetrahydro-4H-chromen-4-one.

Diplosporin D (**8**) had the same molecular formula as compound **7**. Furthermore, compounds **7** and **8** exhibited similar signal patterns in the 1D NMR spectra (Tables 4 and 5). The primary differences between 7 and 8 were the signals for CH-5 [**7**: $\delta_{C/H}$ 70.8/4.51 (d, J = 1.7 Hz); **8**: $\delta_{C/H}$ 73.4/4.27 (d, J = 7.6 Hz)] and CH-6 [**7**: $\delta_{C/H}$ 41.2/1.32 (m); **8**: $\delta_{C/H}$ 36.4/1.97 (m)], suggesting that they shared the same planar structure but had different relative configurations. Additionally, their CD trends were different (Fig. 9). These signals indicated that the absolute configuration of compound **8** was (5*S*,6*R*). Therefore, the structure of **8** was confirmed as (5*S*,6*R*) 6-ethyl-5-methoxy-3-(methoxymethyl)-5,6,7,8-tetrahydro-4*H*-chromen-4-one.

The molecular formula of diclosporin E (**9**) is $C_{11}H_{14}O_3$ according to the HRESIMS result. The 1H NMR and 13C NMR data (Tables 4 and 5) of **9** were similar to those of 6, except for the presence of an additional olefinic methine [$\delta_{C/H}$116.5/6.30 (d, *J* = 5.7 Hz)] and the absence of 3-methoxymethyl, indicating that the methoxymethyl at C-3 in 6 was replaced by a proton in **9**. This modification was the reason for the doublet signal of H-1 [δ_H 7.69 (d, *J* = 5.7 Hz)]. Furthermore, ^{1}H-^{1}H COSY and HMBC correlations (Fig. 10) confirmed the planar structure as 6-ethyl-5-hydroxy-5,6,7,8-tetrahydro-4*H*-chromen-4-one. Moreover, the coupling constant of H-5 (*J* = 7.7 Hz), chemical shifts of related groups (C-4a, CH-5/6, CH_2-7) (Tables 4 and 5), ROESY correlations (Fig. 10), and the CD spectrum for **9** (Fig. 9) closely resembled those of **6**, implying that the absolute configuration of **9** is also (5*S*,6*R*).

Diplosporin F (**10**) was isolated as yellow oils. Its molecular formula is $C_{13}H_{16}O_3$, indicating six degrees of unsaturation. The 1D NMR data also displayed typical signals for a 6-ethyl-3-(methoxymethyl)-4H-chromen-4-one, similar to compounds **5** and **6**. This structural framework accounted for five of the six degrees of unsaturation (Tables 4–6), while the remaining degree of unsaturation is attributed to the presence of a trisubstituted double bond [$\delta_{C/H}$ 111.4/6.37 (s); 140.4]. A detailed analysis of HMBC correlations from H_3-11 to C-6 and H-5 to C-4/C-8a effectively assigned the double bond between C-5 and C-6 (Fig. 11). Therefore, the structure of **10** is 6-ethyl-3-(methoxymethyl)-7,8-dihydro-4H-chromen-4-one.

Diplosporin G (**11**) was obtained as a yellow powder. The molecular formula of compound **11**, $C_{13}H_{14}O_3$, contains two mass units (H2) less than that of **10**. The 1D NMR data of **11** were quite similar to those of **10**, except for the emergence of a disubstituted double bond [$\delta_{C/H}$ 134.0/7.51 (dd, *J* = 8.6, 2.2 Hz); 118.1/7.38

(d, J = 8.6 Hz)] and the disappearance of two methines in **11** (Tables 5 and 6). Additionally, HMBC correlations from H_2-10 to C-5/C-7 indicated that this double bond was located at C7(8) (Fig. 11). This double bond, along with H-5 [δ_H 8.03 (d, J =2.2 Hz)], formed an ABX aromatic coupling system. Therefore, the structure of **11** is 6-ethyl-3-(methoxymethyl)-4H-chromen-4-one.

The molecular formula of **12** is $C_{13}H_{16}O_4$, with six degrees of unsaturation. The similar characteristics of 1D NMR data of **5** and **12** indicate they share the same scaffold. Their 1D NMR data also showed similarity to those of compound **5** (Tables 4–6). In the 1D NMR data, the signals for a terminal olefine [$\delta_{C/H}$ 138.2/6.08 (m); 116.1/5.22 (dd, J = 1.3, 1.3 Hz), 5.19 (dd, J = 1.3, 1.3 Hz)] were observed instead of signals for the methyl triplet at C-11 in **12**, implying that a terminal olefine substituted the ethyl at C-6. The HMBC correlations from H-10 to C-5/C-6/C-7 and the ^{1}H-^{1}H COSY correlations of H_2-11/H-10/H-6/H-5 supported the above deduction (Fig. 11). Considering the similarities in the J value of H-5 (brs), CD spectrum (Fig. 9), and biosynthetic routes of **12** in comparison to **6**, the absolute structure of **12** was determined to be (5*S*,6*R*)-5-hydroxy-3-(methoxymethyl)-6-vinyl-5,6,7,8-tetrahydro-4H-chromen-4-one.

The molecular formula of diplosporin I (**13**) was determined to be $C_{13}H_{18}O_5$ through HRESIMS analysis, which consists of an additional oxygen atom compared to that of **6**. Additionally, the 1D NMR data (Tables 4–6) showed close similarity to those of **6**, implying that **13** is a congener of **11**. The only difference between **6** and **13** is that H-6 in **6** is replaced by a hydroxy in compound **13**. Analysis of the HMBC spectrum of compound **13** enabled the above assignment (Fig. 11). Since no useful ROESY correlations were observed to confirm the relative configuration of compound **13**, calculated 13C NMR and ECD spectra of compound **13** were performed. There are two chiral carbons in compound **13**, so it has two pairs of possible enantiomers, (5*S**, 6*S**)-**13** and (5*S**, 6*R**)-**13**. Firstly, the 13C NMR data of (5*S**, 6*S**)- and (5*S**, 6*R**)-**13** were calculated using GIAO B3LYP/6-31G(d) level in Gaussian 16 and then compared with the experimental data of compound **13**. As shown in Fig. S97 (Supplementary Information), the R2, MAE, and Δ_{max} of the (5*S**, 6*R**)-**13** isomer [R^2= 0.9992, MAE=1.6, Δ_{max} = 2.8 ppm (C-12)] were better than those for the (5*S**, 6*S**)-**13** isomer [R^2=0.9978, MAE= 2.6, Δ_{max} = –7.1 ppm (C-5)] (Supplementary Information), indicating the relative configuration of **13** to be (5*S**, 6*R**). Secondly, the absolute configuration of compound **13** was determined by comparing the calculated ECD with the experimental CD, showing that (5*S*, 6*R*)-**13** exhibited a similar tendency to that shown in Fig. S98 (Supplementary Information). Finally, the structure of

compound **13** was determined to be (5*S*,6*R*)-6-ethyl-5,6-dihydroxy-3-(methoxymethyl)-5,6,7,8-tetrahydro-4*H*-chromen-4-one.

The molecular formula of compound **14** was determined to be $C_{12}H_{14}O_4$ by HRESIMS, suggesting eight degrees of unsaturation. The ^{1}H NMR spectrum (Table 7) displayed distinguished signals for two methoxy (δ_H 3.44 and 3.94), and a set of ABB' coupling benzene system [δ_H 6.82 (d, J = 8.0 Hz); 7.46 (dd, J = 8.0, 8.0 Hz); 6.92 (d, J = 8.0 Hz)]. The ^{13}C NMR spectrum of **14** revealed 12 carbons, which can be assigned to two methoxys (δ_C 56.3, 59.7), one sp^3 methylene (δ_C 31.5), one oxygenated methylene (δ_C 73.6), one oxygenated methine (δ_C 76.3), six aromatic signals (δ_C 111.1, 119.5, 134.7, 114.8, 141.7, 161.4), and one ester carbonyl (δ_C 162.1) (Table 7). The NMR data of **14** resemble those of the known compound **22** (Klaiklay et al. 2012), indicating that compound **14** is also an isocoumarin (Fig. 1). Further analysis of the NMR data and mass spectrometry results between **14** and **22** showed that CH_3-9 in **22** was oxygenated to a methoxymethyl in compound **14**, which was supported by HMBC correlation from CH_3-11 to C-9 (Fig. 11). To determine the absolute configuration of the chiral carbon C-3, the ECD spectra of the two possible conformers of (3*R*)-, and (3*S*)-**14** were calculated. As shown in Fig. S99 (Supplementary Information), the ECD spectrum of (3*S*)-**14** matched better with the experimental one, suggesting that the absolute configuration of C-3 is *S*. Therefore, the structure of **14** is (*S*)-8-methoxy-3-(methoxymethyl)isochroman-1-one.

Besides, 27 known compounds were obtained from three fermentations of rice (**15**–**29**), potato-dextrose-broth (PDB) (**30**-**34**), and glucose-peptone-yeast (GPY) (**24**, **28**, **35**–**41**). Their structures were identified by comparing 1D NMR, MS, and optical data with the reported ones in the literature. As the optical value of compound **26** was close to zero, it was inferred that this compound is a pair of racemates. They were identified as 16-hydroxyisopimar-7-en-19-oic acid (**15**) (Wu et al. 2011), 16-*α*-*D*-mannopyranosyloxyisopimar-7-en-19-oic acid (**16**) (Zhou et al. 2021; Shiono et al. 2009), 16-*α*-*D*-glucopyranosyloxyisopimar-7-en-19-oic acid (**17**) (Zhou et al. 2021; Shiono et al. 2009), cyclo(N-methyl-L-Phe-L-Val-D-Ile-L-Leu-L-Pro) (**18**) (Wu et al. 2011), 5-hydroxy-6-methoxy-2-methyl-4*H*-1-benzopyran-4-one (**19**) (Sun et al. 2012), 5-methoxy-2-methyl-4*H*-1-benzopyran-4-one (**20**) (Teles et al. 2005), 5-hydroxy-8-methoxy-2-methyl-4*H*-1-benzopyran-4-one (**21**) (Sun et al. 2012), (*S*)-8-methoxy-3-methylisochroman-1-one (**22**) [$[\alpha]_D^{23}$ + 211.3 (*c* 0.23, MeOH)] (Klaiklay et al. 2012), (*R*)-(−)-5-

methoxycarbonylmellein (**23**) [[α]$_D^{23}$ + 118.4 (*c* 0.07, MeOH)] (Gonzalez-de-Castro et al. 2014), (*S*)-5-hydroxy-8-methoxy-3-methylisochroman-1-one (**24**) [[α]$_D^{23}$ + 126.2 (*c* 0.02, MeOH)] (Harwood 1983), (*R*)-(−)-5-methoxycarbonylmellein (**25**) [[α]$_D^{23}$ −113.4 (*c* 0.03, MeOH)] (Holker et al. 1981), (±) 8-hydroxy-4-methylisochroman-1-one (**26**) (Sumarah et al. 2011), 5-methoxy-1-naphthnol (**27**) (Si et al. 2011), 1*H*-indole-3-carboxylic acid methyl ester (**28**) (Bao et al. 2007), 22,23-dihydroxyergosta-4,6,8(14)-trien-3-one (**29**) (Lee et al. 2011), (*R*)-5-carboxymellein (**30**) (Xu et al. 2020; Rukachaisirikul et al. 2009), (22*E*,24*R*)-ergosta-7,22-diene-3*β*,5*α*,6*β*-triol (**31**) (Hata et al. 2002), (3*β*,5*α*,6*β*,22*E*)-6-methoxyergosta-7,22-diene-3,5-diol (**32**) (Shimizu et al. 2016), (24*S*)-ergosta-7-ene-3*β*,5*α*,6*β*-triol (**33**) (Gao et al. 2001), 3*β*,5*α*,9*α*-trihydroxy-(22*E*,24*R*)-ergosta-7,22-dien-6-one (**34**) (Wang et al. 2017), 3-methoxy-2-phenethyl-1*H*-pyrrole-1-carbaldehyde (**35**) (Zhou et al. 2018), tryptoline (**36**) (Lu et al. 2010; Airaksinen et al. 1981), cyclo-((*S*)-Pro-(*R*)-Leu)) (**37**) (Yang et al. 2009), 1-phenylethyl-O-*β*-*L*-rhamnopyranoside (**38**) (Wang et al. 2014), 1-phenylethyl-O-*α*-*L*-rhamnopyranoside (**39**) (Chapla et al. 2018), 2-hexylidene-3-methylsuccinic acid (**40**) (Chinworrungsee et al. 2001), and 22,23-dihydroxy-ergosta-4,6,8(14)-trien-3-one-23-*β*-D-glucopyranoside (**41**) (Li et al. 2017).

The metabolites produced by *X. longipes* under three different fermentation conditions exhibit significant variation. The common compounds shared across these conditions are phenylpropanoids and ergosteroids. Phenylpropanoids, a major component of essential oils, are produced by many fungi (Chen et al. 2024). Notably, the addition of 3-methyl-2-butenol to PDB fermentation significantly increased the yield of (*R*)-5-carboxymellein (**30**) to 8.93 mg/L. Ergosteroids, integral components of the fungal cell wall, are consistently co-isolated with other metabolites.

Compared to liquid fermentations, rice fermentation yielded a more diverse array of metabolites, including diterpenoids, cyclic pentapeptides, 2,5-diene-4-pyrane compounds (diplosporins), phenylpropanoids, and ergosteroids. Furthermore, the metabolites from the two liquid fermentations also differed significantly. This suggests that varying fermentation conditions can induce distinct gene expressions, leading to the production of different metabolites.

Previous studies on *X. longipes* GPY cultures identified a series of nor-isopimarane diterpenoids (Chen et al. 2020, 2020). However, no terpenoids were detected in the liquid fermentations in this study, likely due to the addition of 5-carboxymellein, which may inhibit terpenoid synthase activity or gene expression.

Pimarane diterpenoids feature a 6-6-6 fused carbocyclic ring system and are classified into four subclasses: pimarane, isopimarane, ent-pimarane, and *ent*-isopimarane. While most pimarane diterpenoids are found in plants such as *Flickingeria fimbriata*, *Chloranthus henryi*, *Basilicum polystachyon*, and *Sigesbeckia pubescens* (Zhou et al. 2021), only a few have been identified in fungi, including *Xylaria* sp. (Chen et al. 2020, 2020; Masahiko et al. 2014; Shiono et al. 2009; Wang et al. 2021; Zhou et al. 2021), *Acremonium* sp., and *Paraconiothyrium* sp. (Ye and Ai 2022; Zhou et al. 2021).

In *Xylaria* sp., pimarane diterpenoids primarily belong to the isopimarane family. The first 11α,16-epoxy isopimarane (xylarinorditerpene K) is a norisopimarane from GPY fermentation, while 11α,16-epoxy-isopimar-8(9)-en-19β-oic acid (**1**) is a rare normal isopimarane diterpenoid featuring an 11-ether substituent. Typically, isopimarane diterpenoids from *Xylaria* sp. are isolated as glycosides with a sugar moiety at C-16 (Shiono et al. 2009; Wang et al. 2021; Zhou et al. 2021). To date, only two sugar moieties have been reported in these compounds: α-D-mannose and α-D-glucopyranose. Additionally, the double bond in pimarane diterpene glycosides is usually located at C-7(8) (Shiono et al. 2009; Wang et al. 2021; Zhou et al. 2021). However, in the new isopimarane glycosides **2** and **3**, the double bond is positioned at C-8(9).

Macrocyclic peptides from *Xylaria* sp. typically consist of three to six peptides, with cyclic pentapeptides being the most common. So far, fewer than **15** such peptides have been reported from *Xylaria* sp. (Chen et al. 2024). The isolation of compound **4** contributes to the diversity of known cyclopeptides.

Compared to diterpenoids and macrocyclic cyclic peptides, polyketides are the most abundant class of metabolites from *Xylaria* sp. In this study, 19 polyketides were isolated, including nine characterized by a 6-ethyl-4H-chromen-4-one core (diplosporins) (Ibrahim et al. 2014). Notably, nearly all reported diplosporins, including compounds **5**–**8** and **10**–**13**, feature a 3-methoxymethyl group. In contrast, compound **9** lacks this group due to degradation, making it a novel nordiplosporin.

Empirical rules for the configuration of 6-ethyl-5,6,7,8-tetrahydro-4*H*-chromen-4-one

The structural elucidation of natural products continues to pose significant challenges in chemical research. The development of advanced methodologies, including *J*-based configuration analysis (JBCA), nuclear Overhauser effect spectroscopy, quantum-chemical calculations, X-ray crystallographic analysis, and the establishment of empirical NMR data rules, has proven effective in determining both relative and absolute configurations of organic molecules. While the planar structures of most small molecules can be reliably

641 determined through NMR spectroscopy coupled with mass spectrometry, the determination of
642 stereochemical configurations remains challenging due to the structural diversity of chiral centers and the
643 difficulties in obtaining suitable single crystals for diffraction analysis. Consequently, identifying
644 characteristic NMR and/or circular dichroism (CD) patterns for specific compound classes has emerged as
645 a valuable and efficient supplementary approach for absolute configuration determination.

646 In the present study, a series of diplosporins were isolated from the rice fermentation products of *X.*
647 *longipes*. While determining their absolute configurations, distinct J-coupling constants and CD spectra
648 patterns were identified and systematically characterized. As illustrated in Figs. 8 and 9, the coupling
649 constants between H-5 and H-6 ($J_{H\text{-}5/H\text{-}6}$) provided crucial information about their spatial orientation.
650 Specifically, small coupling constants (J < 3.0 Hz) indicated identical orientations of H-5 and H-6, while
651 larger values suggested different orientations. Furthermore, the CD spectral patterns exhibited characteristic
652 trends: a "valley-to-peak" sequence indicated α-orientation of both H-5 and H-6, whereas the reverse pattern
653 suggested β-orientation of H-5 and α-orientation of H-6 (Fig. 9).

654 **Biological properties**

655 Building on previous reports of immunosuppressive activities of diterpenoids from *X. longipes* against the
656 proliferation of induced T and B lymphocytes, all compounds in this study were evaluated for their anti-
657 proliferative effects on ConA-induced T lymphocytes and LPS-induced B lymphocytes. As summarized in
658 Table 8, compounds **32** and **41** exhibited significant suppressive activity against ConA-induced T
659 lymphocytes, with IC_{50} values of 3.1 and 12.1 μM, respectively. Additionally, compounds **10**, **11**, **32**, **36**, and
660 **41** demonstrated inhibitory effects on LPS-induced B lymphocytes, with IC_{50} values ranging from 8.0 to
661 20.0 μM. The positive control, Dexamethasone (Dex), showed IC_{50} values of 1.9 and 1.0 μM, respectively.
662 Notably, all active compounds displayed CC_{50} values exceeding 20.0 μM, indicating a superior safety profile
663 compared to Dex. In contrast, isopimarane diterpenoids **1**–**3** and **15**–**17** did not exhibit significant
664 suppressive activity against either ConA-induced T lymphocytes or LPS-induced B lymphocytes.

665 Given the reported lack of cytotoxicity of nor-isopimarane diterpenoids against T and B lymphocytes at
666 40 μM (Chen et al., 2020), the inhibition rates of compounds **1**–**3** and **15**–**17** were further evaluated at two
667 concentrations (40.0 and 20.0 μM). As shown in Table 9, these diterpenoids displayed dose-dependent
668 suppression of cell proliferation in both ConA-induced T lymphocytes and LPS-induced B lymphocytes,

669 with compounds **2** and **15** showing particularly notable activity. Concurrently, high cell viability (Table 9)
670 confirmed that diterpenoids **1**–**3** and **15**–**17** were non-toxic at the cellular level, further supporting their
671 safety profile.

672 Considering the notable immunosuppressive activity of compounds **2** and **32**, which possess distinct
673 structural scaffolds, their inhibitory effects were further investigated using EdU (5-ethynyl-2'-deoxyuridine)
674 imaging kits (HF488). The EdU assay, which detects proliferating cells, revealed that lymphocyte
675 proliferation (indicated by green fluorescence) was markedly enhanced in the model group (Mod) following
676 stimulation with ConA and LPS compared to the control group (Con). In contrast, treatment with compounds
677 **2** and **32** significantly suppressed the proliferation of induced T and B cells relative to the model group (Figs.
678 12A and 12B).

679 Additionally, compounds **2**, **15**, and **32** were evaluated for their ability to inhibit the secretion of cytokines
680 interferon (IFN)-γ, interleukin (IL)-2, and IL-17A in mouse splenocytes, following established protocols
681 (Jing et al., 2021; Zhao et al., 2024). As illustrated in Fig. 12C, the levels of IFN-γ, IL-2, and IL-17A were
682 significantly elevated in the model group compared to the control group ($P < 0.0001$). Treatment with
683 compounds **2**, **15**, and **32** resulted in a significant reduction in IFN-γ secretion across all sample groups ($P <$
684 0.0001). While these compounds also decreased the secretion of IL-2 and IL-17A, most sample groups did
685 not show statistically significant differences compared to the model group. Notably, compound **15** (40 μM)
686 significantly reduced IL-2 levels ($P < 0.01$), while compounds **2** (40 μM) and **32** (10 μM) markedly lowered
687 IL-17A levels ($P < 0.05$ and $P < 0.01$, respectively). Given the established role of IFN-γ in T-cell proliferation
688 (Liu et al., 2022), the antiproliferative effects of compounds **2**, **15**, and **32** on T lymphocytes may be mediated,
689 at least in part, through the suppression of IFN-γ secretion.

690 Furthermore, all isolated compounds (**1–41**) were assessed for their antiproliferative activity against the
691 HaCaT cell line, an immortalized keratinocyte model. As summarized in Table 10, compounds **9**, **10**, **13**, **19**,
692 **22**, **24**, **25**, **28**, **30**, **32–35**, and **37–41** exhibited inhibitory effects on HaCaT cell proliferation, with IC_{50}
693 values ranging from 25.2 to 35.1 μM. Notably, the IC_{50} value of the positive control, Methotrexate (MTX),
694 was 26.4 μM. Complementary EdU experiments (Fig. 13) corroborated these findings, demonstrating that
695 the proliferation rates of HaCaT cells in sample groups treated with compounds **10**, **19**, **23**, **32**, **38**, and **41**
696 were significantly reduced compared to the control group, consistent with the results obtained from the CCK-

8 assay.

Nuclear factor-κB (NF-κB), a family of heterodimeric proteins comprising the p50 and p65 subunits, is critical in regulating cellular proliferation, differentiation, and survival (Hexum et al., 2012). Since compounds **10** and **32** demonstrated inhibitory effects on the proliferation of induced T/B lymphocytes and HaCaT cells, their molecular mechanisms were further investigated concerning the NF-κB pathway. As shown in Fig. 14, compounds **10** (31.0 μM) and **32** (27.0 μM) significantly attenuated NF-κB activation, with P values of less than 0.0001 and 0.01, respectively.

Psoriasis, a chronic inflammatory skin disorder affecting 2–3% of the global population, remains without a definitive cure (Dai et al., 2024). The pathophysiology of psoriasis is characterized by the hyperproliferation of keratinocytes, driven by excessive pro-inflammatory cytokines such as IFN-γ and IL-17A, which are predominantly secreted by activated T cells, particularly Th17 cells (Castaldo et al., 2021; Rendon and Schäkel, 2019). Given that compound **32** effectively suppressed the proliferation of induced T lymphocytes and HaCaT cells and the secretion of key cytokines (IFN-γ and IL-17A), it emerges as a promising candidate for further investigation as a potential therapeutic agent for psoriasis.

Analysis of the structure-activity relationship

For immunosuppressive activity, compounds **10**, **11**, **32**, **36**, and **41** demonstrated notable efficacy, representing three structural classes: diplosporins (**10**, **11**), an indole alkaloid (**36**), and ergosterols (**32**, **41**). Ergosterols, along with Dex, belong to the steroid family. The inhibitory effects of compounds **32** and **41** on the proliferation of induced T and B lymphocytes can be attributed to their steroid nucleus. Notably, the activities of compounds **32** and **41** surpassed those of their analogs **31** and **29**, respectively, suggesting that the OCH_3-6 group in **32** and the 23-glucopyranosyl moiety in **41** are critical functional groups for enhancing immunosuppressive activity.

Compounds **10**, **11**, and **36** exhibited significant selectivity in inhibiting LPS-induced B lymphocyte proliferation. Among the diplosporins, the presence of a double bond at C5(6) in compounds **10** and **11** appears to be a key structural feature contributing to their immunosuppressive activity. As shown in Table 8, compound **10** displayed superior activity compared to compound **11**, indicating that higher degrees of unsaturation may negatively impact the immunosuppressive efficacy of these compounds.

Conclusion

The *Xylaria* genus, a widely distributed filamentous fungus found in marine and terrestrial environments, is known for producing diverse secondary metabolites. A comprehensive phytochemical investigation of three fermentation cultures of *X. longipes* led to the isolation of 41 metabolites, including 14 novel compounds (**1**−**14**). These metabolites encompassed a variety of structural classes, such as isopimarane-type diterpenoids, isopimarane-type diterpenoid glycosides, cyclic peptides, polyketides, phenylpropanoids, pyrroles, and ergosterols. Notably, a shift in the production of secondary metabolites was observed when transitioning from solid (rice) to liquid media (PDB and GPY, both supplemented with 3-methyl-2-butenol), highlighting the media-dependent nature of metabolite biosynthesis. This study also validated the utility of combining ^{3}J coupling constants with circular dichroism (CD) trends for determining the absolute configurations of C-5 and C-6 in diplosporins.

All isolated compounds were evaluated for their anti-proliferative activity against ConA-induced T lymphocytes, LPS-induced B lymphocytes, and HaCaT cells *in vitro*, with several compounds demonstrating significant activity. Ergosteroids **32** and **41** exhibited potent immunosuppressive and antiproliferative effects against HaCaT cells while maintaining high lymphocyte safety. Cytokine analysis revealed that active compounds **2**, **15**, and **32** significantly reduced IFN-γ levels, with compound **32** (10 μM) also inhibiting IL-17A secretion. Further immunofluorescence assays indicated that the antiproliferative effects of compounds **10** and **32** on HaCaT cells were mediated, at least in part, through the inactivation of NF-κB via reduced phosphorylation of p65. Given its multifaceted activities, compound **32** is a promising candidate for developing therapeutic agents for psoriasis.

Supplementary Information

The online version contains supplementary material available at https:// doi.org/XXX, including the NMR, HRMS data, computational details, and other relevant information on compounds **1**–**14**, together with all the obtained sequences deposited in GenBank.

Adherence to national and international regulations

Not applicable.

Authors' contributions

ZZZ, XP, and WSF conceived and designed the experiments. YW, LLW, and MJS performed all experiments and contributed to the data acquisition. XYW, JKW, ZZW, and YW performed all data analyses. ZZZ wrote the original manuscript. All authors reviewed and improved the manuscript and have agreed to the published version of the manuscript.

Funding

This work was supported by the National Natural Science Foundation of China (82003607, 82274114), the Excellent Young Scientists Fund of the Natural Science Foundation of Henan Province (242300421091), Natural Science Foundation of Henan (CN) (232301420094), Henan Postdoctoral Research Foundation (CN) (HN2022078), Scientific and Technological Key Project in Henan Province (CN) (242102310567, 242102311289), Science and Technology Innovative Research Team in Higher Educational Institutions of Henan Province (CN) (24IRTSTHN039), Scientific Research Nursery Project of Henan University of Chinese Medicine (CN) (MP2024-10).

Availability of data and materials

Not applicable.

Declarations

Ethics approval and consent to participate

The animal study (No. DWLL202003116) was reviewed and approved by the Animal Welfare Ethics Committee of the Henan University of Chinese Medicine.

Consent for publication

Not applicable.

Competing interests

The authors declare that they have no competing interests.

References

Airaksinen MM, Kari I (1981) *β*-carbolines, psychoactive compounds in the mammalian body. Part I: Occurrence, origin and metabolism. Med Biol 59(1):21–34.

Bao B, Zhang P, Lee Y, et al (2007) Monoindole alkaloids from a marine sponge *Spongosorites* sp. Mar Drugs 5(2):31–39. https://doi.10.3390/md502031

Biram A, Shulman Z (2020). Evaluation of B Cell proliferation in *vivo* by EdU incorporation assay. Bio Protoc 10: e3602. https://doi.10.21769/BioProtoc.3602

Bode HB, Bethe B, Höfs R, Zeeck A (2002) Big effects from small changes: possible ways to explore nature's chemical diversity. Chembiochem 3(7):619–27. https://doi.10.1002/1439-7633(20020703)3:7<619::AID-CBIC619>3.0.CO;2-9

Bruhn T, Schaumlöffel A, Hemberger Y, Bringmann G (2012) Spec Dis, version 1.71, University of Würzburg, Germany.

Castaldo G, Pagano I, Grimaldi M et al (2021) Effect of very-low-calorie ketogenic diet on psoriasis patients: A nuclear magnetic resonance-based metabolomic study. J Proteome Res 20(3):1509–1521. https://doi.10.1021/acs.jproteome.0c00646

Chapla VM, Zeraik ML, Cafeu MC et al (2018) Griseofulvin, diketopiperazines and cytochalasins from endophytic fungi *Colletotrichum crassipes* and *Xylaria* sp., and their antifungal, antioxidant and anticholinesterase activities. J Brazil Chem Soc 29(8):1707–1713. https://doi.10.21577/0103-5053.20180045

Chen HP, Li J, Zhao ZZ et al (2020) Diterpenes with bicyclo[2.2.2]octane moieties from the fungicolous fungus *Xylaria longipes* HFG1018. Org Biomol Chem 18(13):2410–2415. https://doi.10.1039/d0ob00220h

Chen HP, Zhao ZZ, Cheng GG et al (2020) Immunosuppressive nor-isopimarane diterpenes from cultures of the fungicolous fungus *Xylaria longipes* HFG1018. J Nat Prod 83(2):401–412. https://doi.org/10.1021/acs.jnatprod.9b00889

Chen W, Yu M, Chen S et al (2024) Structures and biological activities of secondary metabolites from *Xylaria* spp. J Fungi 10(3):190. https://doi.10.3390/jof10030190

Chinworrungsee M, Kittakoop P, Isaka M et al (2001) Antimalarial halorosellinic acid from the marine fungus *Halorosellinia*

oceanica. Bioorg Med Chem Lett 11(15):1965–1969. https://doi.10.1016/s0960-894x(01)00327-4

Dai X, Permana AD, Li M et al (2024) Calcipotriol nanosuspension-loaded trilayer dissolving microneedle patches for the treatment of psoriasis: *In vitro* delivery and *in vivo* antipsoriatic activity studies. Mol Pharm 21(6):2813–2827. https://doi.10.1021/acs.molpharmaceut.3c01223

Franco MEE, Wisecaver JH, Arnold AE, Ju YM, Slot JC, Ahrendt S, Moore LP, Eastman KE, Scott K, Konkel Z, Mondo SJ, Kuo A, Hayes RD, Haridas S, Andreopoulos B, Riley R, LaButti K, Pangilinan J, Lipzen A, Amirebrahimi M, Yan J, Adam C, Keymanesh K, Ng V, Louie K, Northen T, Drula E, Henrissat B, Hsieh HM, Youens-Clark K, Lutzoni F, Miadlikowska J, Eastwood DC, Hamelin RC, Grigoriev IV, U'Ren JM (2022) Ecological generalism drives hyperdiversity of secondary metabolite gene clusters in xylarialean endophytes. New Phytol 233(3):1317-1330. https://doi.10.1111/nph.17873.

Frisch MJ, Trucks GW, Schlegel HB et al (2016) Gaussian, Inc., Wallingford CT.

Gao JM, Dong ZJ, Liu JK (2001). A new ceramide from the basidiomycete *Russula cyanoxantha*. Lipids 36(2):175–181. https://doi.10.1007/s11745-001-0704-x

Gonzalez-de-Castro A, Robertson CM, Xiao J (2014) Dehydrogenative α-oxygenation of ethers with an iron catalyst. J Am Chem Soc 136(23):8350–8360. https://doi.10.1021/ja502167h

Harwood LM (1983) An investigation into the regioselectivity of the acid catalysed Claisen rearrangement of methyl 4-and 5-allyloxy-2-hydroxybenzoate and derivatives. J Am Chem Soc Chem Commun (9):530–532. https://doi.10.1039/C39830000530

Hata K, Sugawara F, Ohisa N, et al (2002) Stimulative effects of (22*E*,24*R*)-ergosta-7,22-diene-3β,5α,6β-triol from fruiting bodies of *Tricholoma auratum*, on a mouse osteoblastic cell line, MC3T3-E1. Biol Pharm Bull 25(8):1040–1044. https://doi.10.1248/bpb.25.1040

Hexum JK, Tello-Aburto R, Struntz NB et al (2012) Bicyclic cyclohexenones as inhibitors of NF-κB signaling. ACS Med Chem Lett 3:459–464.https://doi.10.1021/ml300034a

Holker JSE, Simpson TJ (1981) Studies on fungal metabolites. Part 2. Carbon-13 nuclear magnetic resonance biosynthetic studies on pentaketide metabolites of *Aspergillus melleus*: 3-(1,2-epoxypropyl)-5,6-dihydro-5-hydroxy-6-methylpyran-2-one and mullein. J Am Chem Soc Perkin Transactions 1:1397–1400.

Ibrahim A, Sørensen D, Jenkins HA et al (2014) New diplosporin and agistatine derivatives produced by the fungal endophyte *Xylaria* sp. isolated from *Vitis labrusca*. Phytochemistry Lett 9:179–183. http://dx.doi.org/10.1016/j.phytol.2014.06.011

Jing SX, Fu R, Li CH et al (2021) Immunosuppresive sesterterpenoids and norsesterterpenoids from *Colquhounia coccinea* var. *mollis.* J Org Chem 86: 11169−11176. https://doi.10.1021/acs.joc.1c00374

Klaiklay S, Rukachaisirikul V, Sukpondma Y et al (2012) Metabolites from the mangrove-derived fungus *Xylaria cubensis* PSU-MA34. Arch Pharm Res 35(7):1127–1131. https://doi.10.1007/s12272-012-0701-y

Lee IS, Kim JP, Na MK et al (2011) Cytotoxicity of ergosterol derivatives from the fruiting bodies of *Hygrophorus russula*. Nat Prod Sci 17(2):85–89.

Li W, Yang XQ, Yang YB et al (2017) A novel steroid derivative and a new steroidal saponin from endophytic fungus *Xylaria* sp. Nat Prod Commun 12(6):901–904.

Li YY, Hu ZY, Shen YM (2011) Two new cyclopeptides and one new nonenolide from *Xylaria* sp. 101. Nat Prod Commun 6(12):1843–1846.

Liu W, Zhang S, Wang (2022) J IFN-γ, should not be ignored in SLE. Front Immunol 13: 954706. https://doi.10.3389/fimmu.2022.954706

Lu YN, Pan CQ, Xi DY et al (2010) Alkaloids from the sea anemone *Haliplanella luciae*. Chin J Mar Drugs 29(1):45–49. https://doi.10.3724/SP.J.1231.2010.06703

Masahiko I, Arunrat Y, Sumalee S et al (2014) Isopimaranes and eremophilanes from the wood-decay fungus *Xylaria allantoidea* BCC 23163. Phytochemistry Lett 8:59–64. http://dx.doi.org/10.1016/j.phytol.2014.06.011

Pan R, Bai X, Chen J et al (2019) Exploring structural diversity of microbe secondary metabolites using OSMAC strategy: A literature review. Front Microbiol 10:294. https://doi.10.3389/fmicb.2019.00294

Pfütze S, Charria-Girón E, Schulzke E et al (2024) Depicting the chemical diversity of bioactive meroterpenoids produced by the largest organism on earth. Angew Chem Int Ed Engl. 63(16):e202318505. https://doi.10.1002/anie.202318505

Rendon A, Schäkel K (2019) Psoriasis pathogenesis and treatment. Int J Mol Sci 20:1475. https://doi.org/10.3390/ijms20061475

Rukachaisirikul V, Khamthong N, Sukpondma Y et al (2009) An [11]cytochalasin derivative from the marine-derived fungus *Xylaria* sp. PSU-F100. Chem Pharm Bull (Tokyo) 57(12):1409–1411. https://doi.10.1248/cpb.57.1409

Shimizu T, Kawai J, Ouchi K et al (2016) Agarol, an ergosterol derivative from *Agaricus blazei*, induces caspase-independent apoptosis in human cancer cells. Int J Oncol 48(4):1670–1678. https://doi.10.3892/ijo.2016.3391

Shiono Y, Motoki S, Koseki T et al (2009) Isopimarane diterpene glycosides, apoptosis inducers, obtained from fruiting bodies of the ascomycete *Xylaria polymorpha*. Phytochemistry 70(7):935–939. https://doi.10.1016/j.phytochem.2009.03.023

Si CL, Zhang Y, Zhu ZY et al (2011) Chemical constituents with antioxidant activity from the pericarps of *Juglans sigillata*. Chem Nat Compd 47:442–445. https://doi.10.1007/s10600-011-9956-7

Sumarah MW, Puniani E, Blackwell BA, Miller JD (2008). Characterization of polyketide metabolites from foliar endophytes of *Picea glauca*. J Nat Prod 71(8):1393–1398. https://doi.10.1021/np800192f

Sun JZ, Liu XZ, Mckenzie EHC et al (2019) Fungicolous fungi: Terminology, diversity, distribution, evolution, and species checklist. Fungal Divers 95:337–430. https://doi.10.1007/s13225-019-00422-9

Sun YW, Liu GM, Huang H, Yu PZ (2012) Chromone derivatives from *Halenia elliptica* and their anti-HBV activities. Phytochemistry 75:169–176. https://doi.10.1016/j.phytochem.2011.09.015

Teles HL, Silva GH, Castro-Gamboa I et al (2005) Benzopyrans from *Curvularia* sp., an endophytic fungus associated with *Ocotea corymbosa* (Lauraceae). Phytochemistry 66(19):2363–2367. https://doi.10.1016/j.phytochem.2005.04.043

Wang F, Han S, Hu S et al (2014) Two new secondary metabolites from *Xylaria* sp. cfcc 87468. Molecules 19(1):1250–1257. https://doi.10.3390/molecules19011250

Wang J, Zhang Z, Wang Y et al (2017) Chemical constituents from mycelia and spores of fungus *Cordyceps cicadae*. Chin Herb Med 9(2):188–192. https://doi.10.1016/S1674-6384(17)60094-7

Wang QY, Chen HP, Liu JK (2021) Isopimarane diterpenes from the rice fermentation of the fungicolous fungus *Xylaria longipes* hfg1018. Phytochemistry Lett 45:100–104. https://doi.org/10.1016/j.phytol.2021.08.005

Wu W, Dai H, Bao L et al (2011) Isolation and structural elucidation of proline-containing cyclopentapeptides from an endolichenic *Xylaria* sp. J Nat Prod 74(5):1303–1308. https://doi.10.1021/np100909y

Xu ZL, Zheng N, Cao S, et al (2020) Secondary metabolites from the endophytic fungus *Stemphylium lycopersici* and their antibacterial activities. Chem Nat Compd 56(6):1162–1165. https://doi.10.1007/s10600-020-03256-z

Yang B, Dong J, Zhou X et al (2009) Proline-containing dipeptides from a marine sponge of a *Callyspongia* Species. Helvetica Chimica Acta 92(6):1112–1117. https://doi.10.1002/hlca.200800422

Ye K, Ai HL (2022) Pimarane diterpenes from fungi. Pharmaceuticals (Basel) 15(10):1291. https://doi.10.3390/ph15101291. https://doi.10.3390/ph15101291

Zhang H, Deng Z, Guo Z et al (2015) Effect of Culture Conditions on Metabolite Production of *Xylaria* sp. Molecules 20(5):7940-50. https://doi.10.3390/molecules20057940

Zhang D, Gao F, Jakovlić I, Zou H, Zhang J, Li WX, Wang GT (2020) PhyloSuite: An integrated and scalable desktop platform for streamlined molecular sequence data management and evolutionary phylogenetics studies. Mol Ecol Resour 20(1):

348-355. https://doi.10.1111/1755-0998.

Zhao ZZ, Liang XB, He HJ et al (2024) Diterpenoids with potent anti-psoriasis activity from *Euphorbia helioscopia* L. Molecules 29(17): 4104. https://doi.10.3390/molecules29174104

Zhao ZZ, Zhang F, Ji BY et al (2023). Pyrrole alkaloids from the fruiting bodies of edible mushroom *Lentinula edodes.* RSC adv 13:18223–18228. https://doi.10.1039/d3ra02672h

Zhou P, Zheng M, Li XN et al (2021) Hypoxylonoids A-G: Isopimarane diterpene glycosides from *Xylaria hypoxylon*. Phytochemistry 182:112613. https://doi.10.1016/j.phytochem.2020.112613

Zhou M, Zhang RQ, Chen YJ et al (2018) Three new pyrrole alkaloids from the roots of *Lepidium meyenii*. Phytochem Lett 23:137–140. https://doi.10.1016/j.phytol.2017.12.002

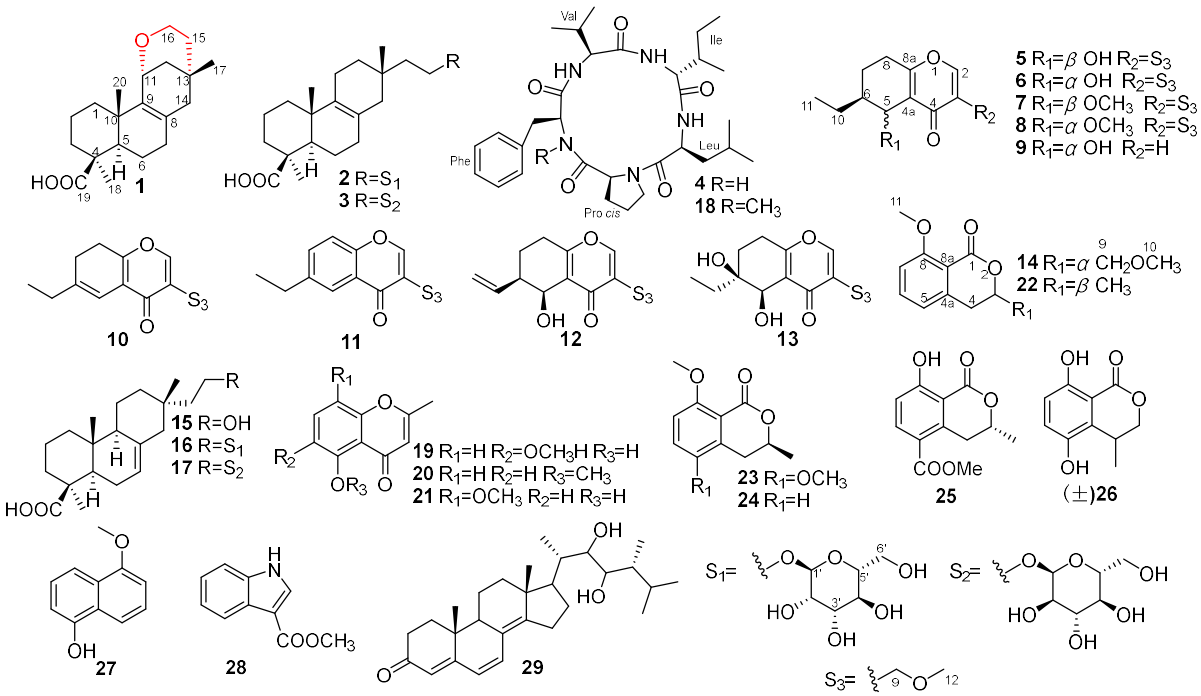

888
889 **Fig. 1** The structures of compounds **1**–**29** from the rice fermentation of *X. longipes* HFG1018.

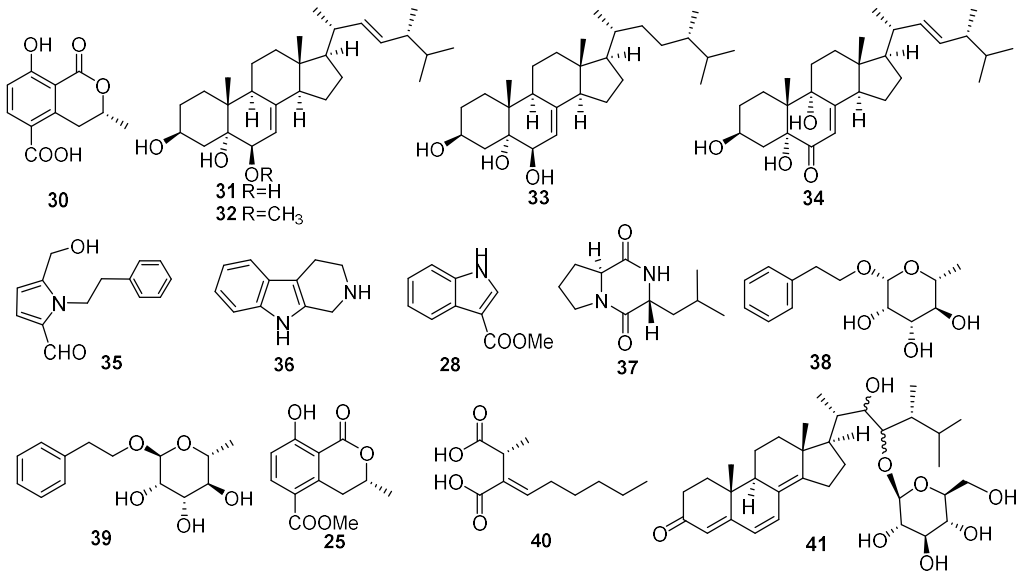

890
891 **Fig. 2** The structures of compounds **30**–**34** (PDB) and **35**–**41** (GPY) from liquid fermentations of *X.*
892 *longipes* HFG1018.
893

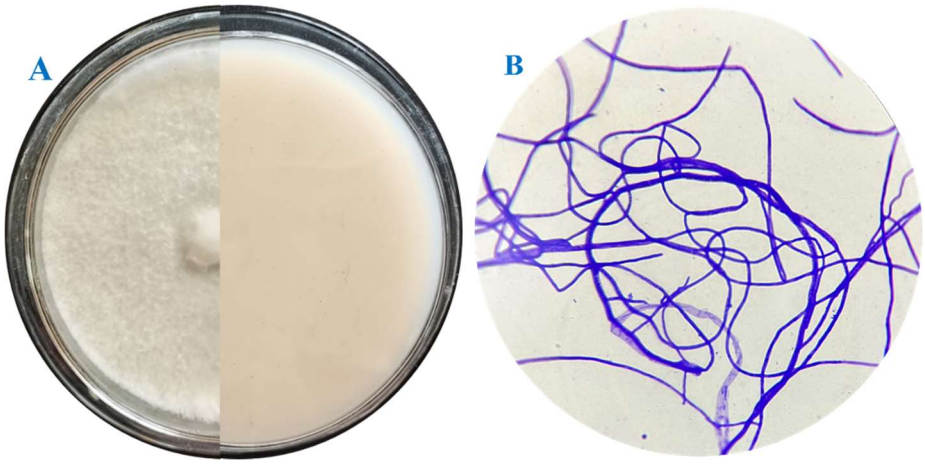

Fig. 3 The phenotypical and morphological characters of *Xylaria longipes* HFG1018. (A) The colony. (B) Methylene blue-stained Mycelium (100 ×).

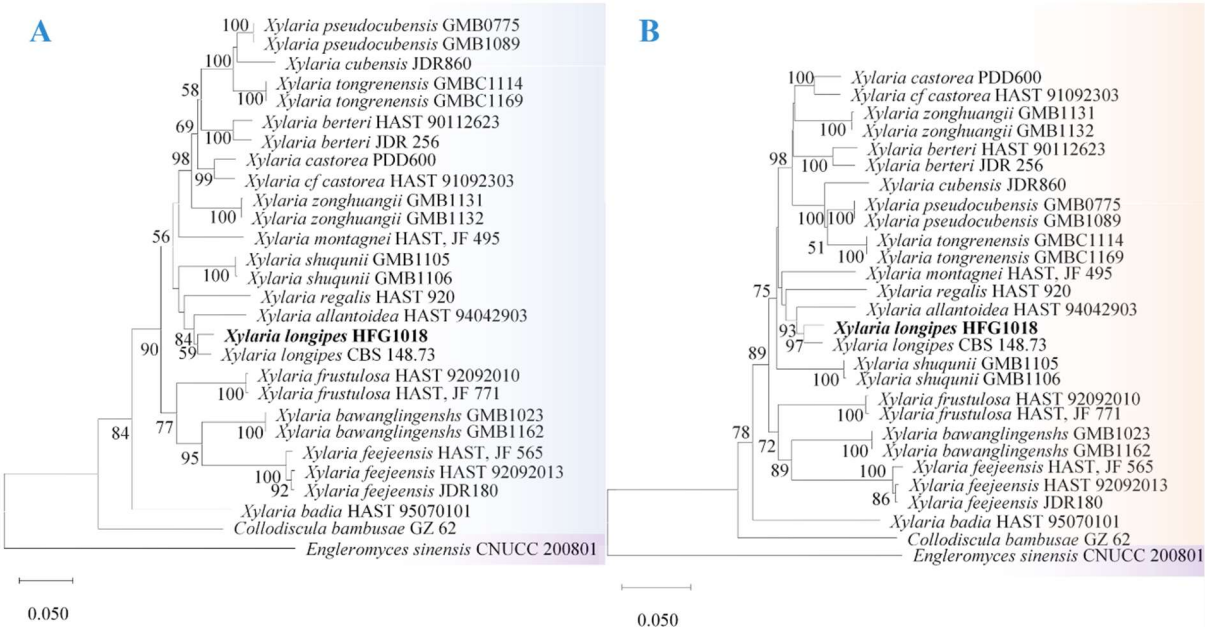

Fig. 4 Maximum likelihood trees of *Xylaria* constructed using internal transcribed spacer (ITS), *β*-tubulin gene (TUB2), and DNA-directed RNA Polymerase II subunit 2 (rpb2) gene sequence data sets. Bootstrap support values of maximum likelihood (MLBP) above 50% are shown at the nodes. The tree was rooted to *Engleromyces sinensis* CNUCC 200801. The strain *Xylaria longipes* described species are marked in bold. (A) ML tree. (B) NJ tree.

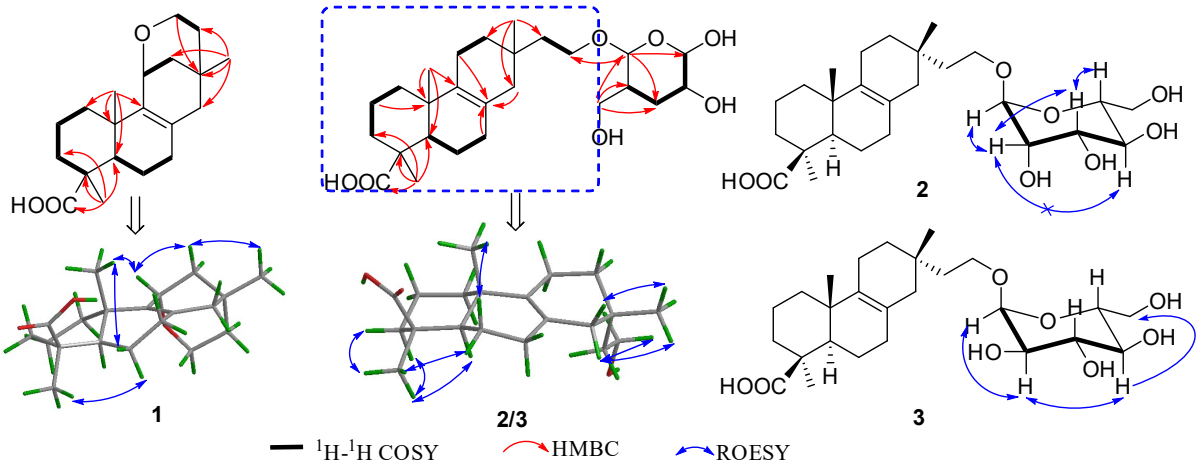

Fig. 5 Key 2D NMR correlations of compounds **1**–**3**.

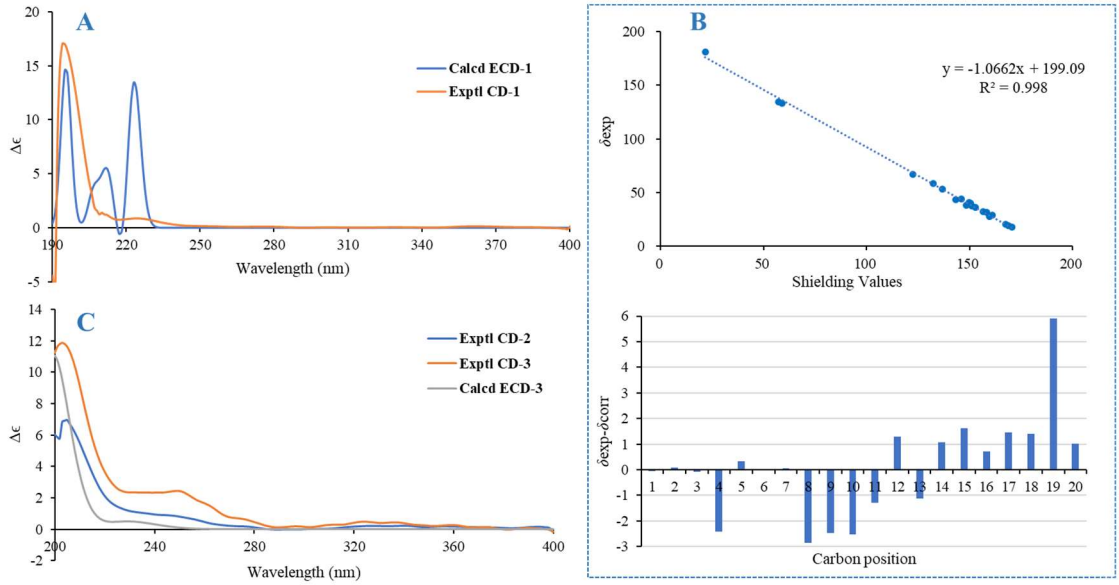

Fig. 6 (A) Comparison of the calculated ECD spectrum for **1** (σ = 0.10 eV, and UV shift 5 nm) with its experimental CD spectrum in MeOH; (B) Comparison of the calculated ^{13}C NMR data for **1** with its experimental spectrum in $CDCl_3$; (C) Comparison of the calculated ECD spectrum for **2**, **3** (σ = 0.30 eV, and UV shift 7 nm) with their experimental CD spectra in MeOH.

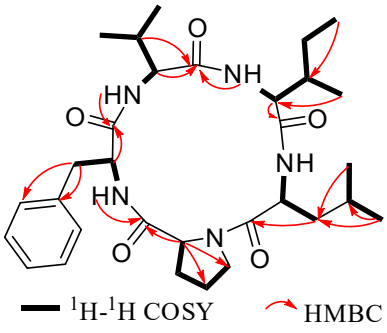

Fig. 7 Key HMBC correlations of compound **4**.

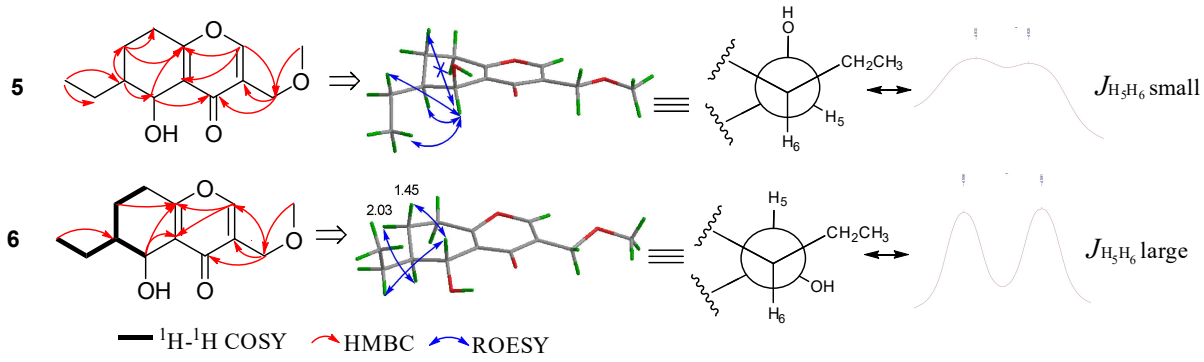

Fig. 8 Key 2D NMR correlations, stereochemistry analysis, and ^{1}H NMR spectral comparison of compounds **5** and **6**.

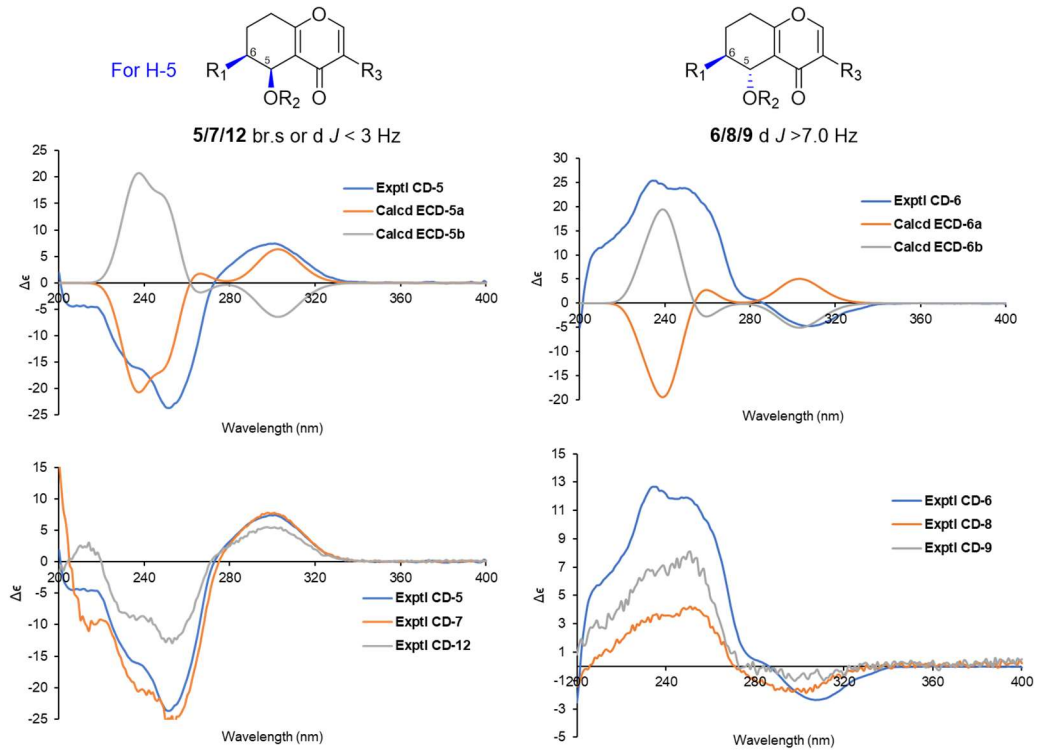

Fig. 9 Comparison of the calculated ECD spectrum for **5** (σ = 0.20 eV, UV shift 7 nm), **6** (σ = 0.22 eV, UV shift 9 nm) with their experimental spectra in MeOH; Empirical rules for configuration of diplosporins.

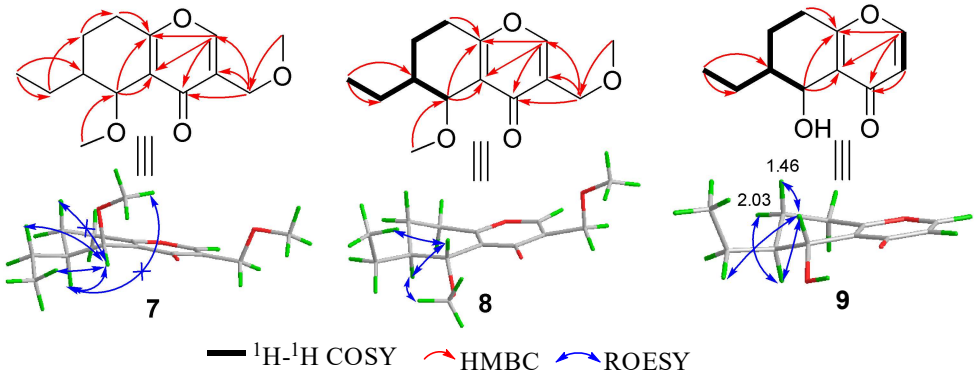

Fig. 10 Key 2D NMR correlations of compounds **7**–**9**.

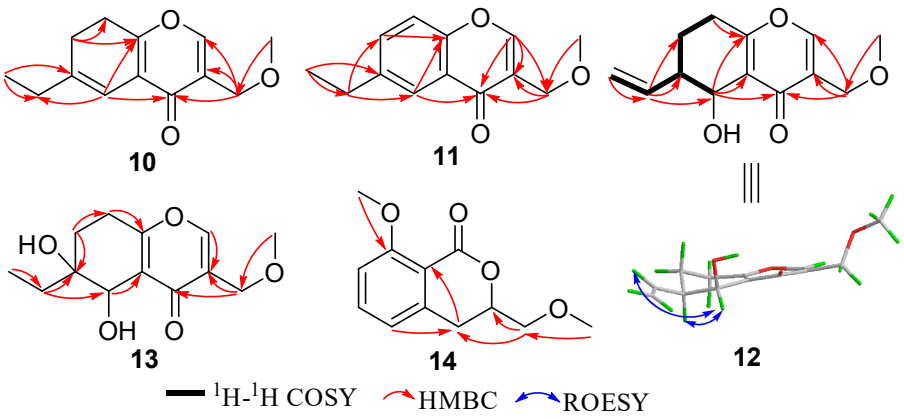

Fig. 11 Key 2D NMR correlations of compounds **10**–**14**.

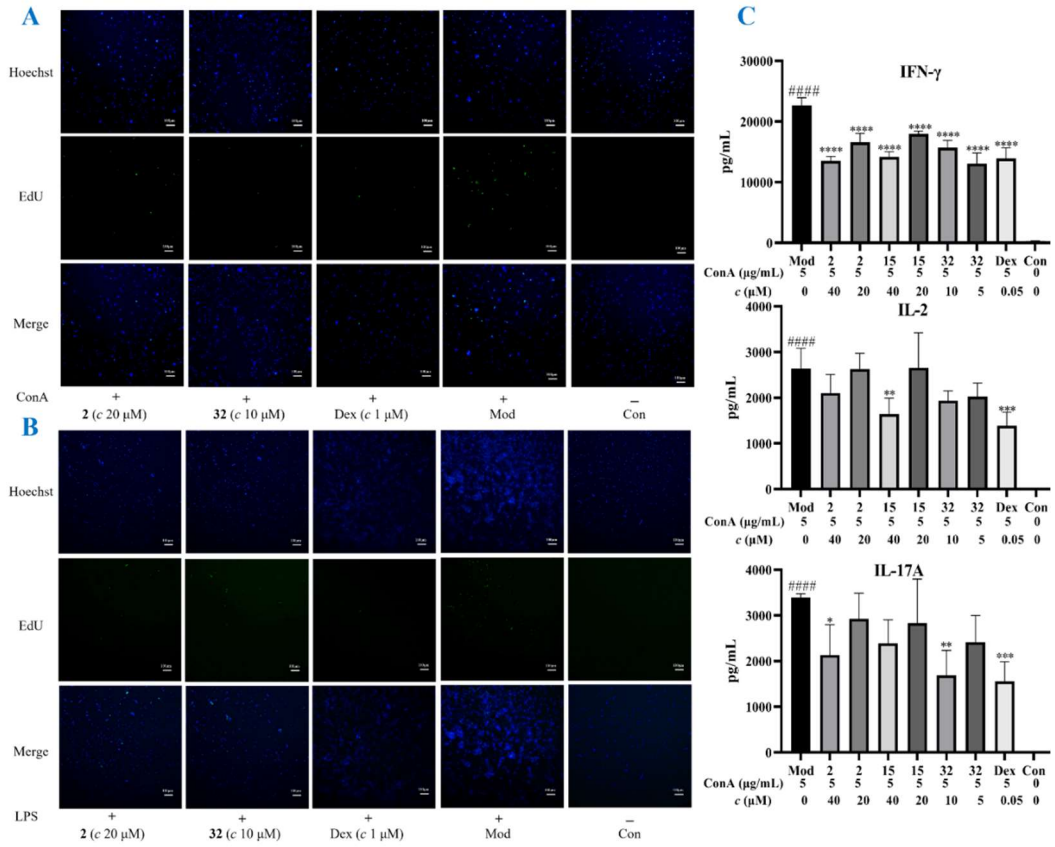

Fig. 12 (A/B) Inhibitory activities of compounds **2** ($c = 20\ \mu$M), **32** ($c = 10\ \mu$M), and Dex ($c = 2, 1\ \mu$M) against induced T cells (Con A 5 μg/mL) and B (LPS 15 μg/mL) cells measured by EdU. (C) Concentrations of IFN-γ, IL-2, and IL-17A of induced T cells (Con A 5 μg/mL) in different groups (*vs* Con $^{\#\#\#\#}P < 0.0001$; *vs* Mod, **** $P < 0.0001$, ** $P < 0.01$, * $P < 0.05$).

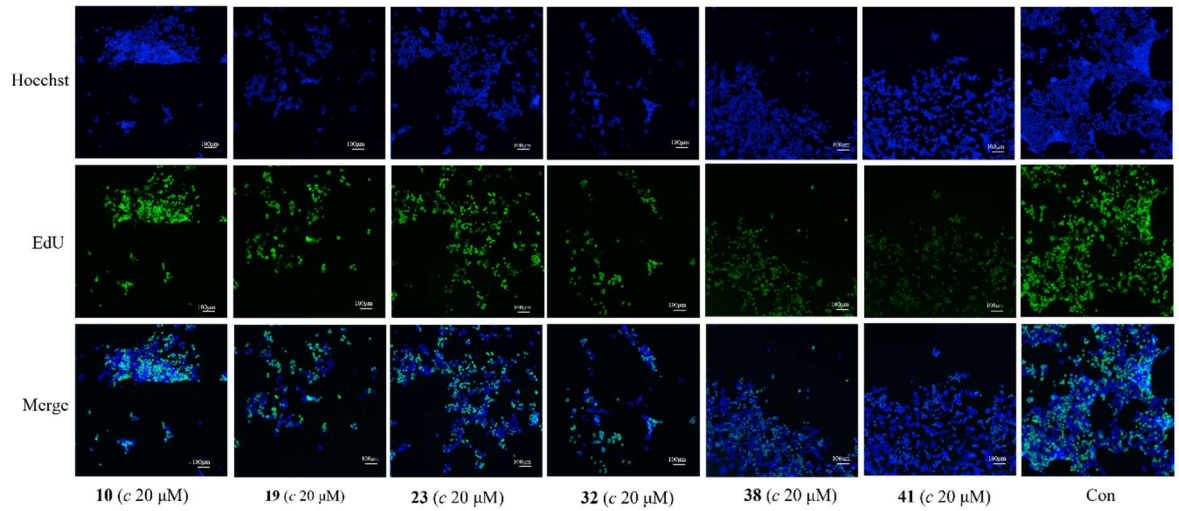

Fig. 13 Inhibitory activities of compounds **10**, **19**, **23**, **32**, **38**, and **41** (c =20 μM), against HaCaT cells measured by EdU.

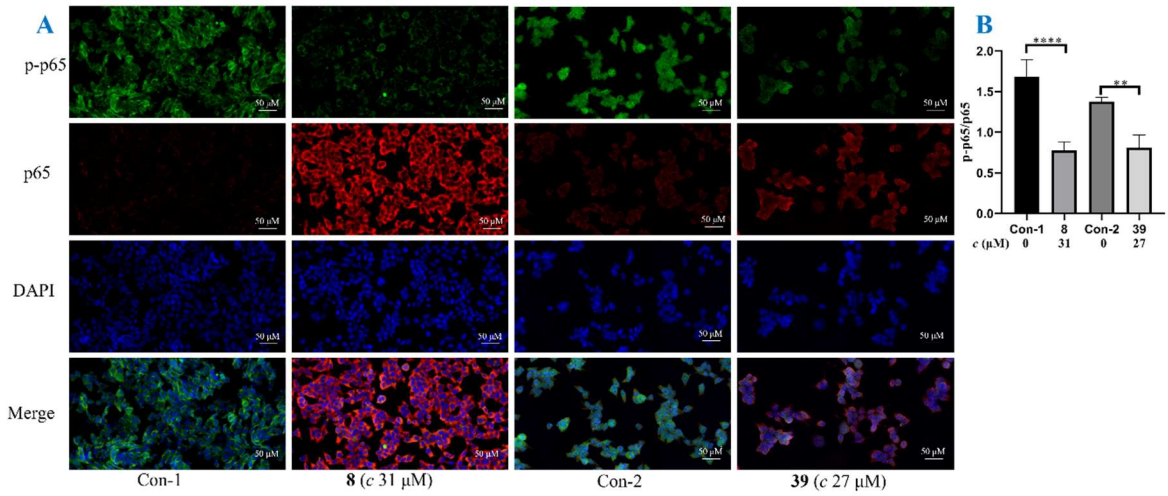

Fig. 14 (A) Immunofluorescence images: Effects of compounds **10** (c =31 μM) and **32** (c =27 μM) on p-p65 and p65 expression levels in HaCaT cells. (B) Ratios of p-p65/p65 of HaCaT cells in different groups (*vs* Con, **** $P < 0.0001$, ** $P < 0.01$).

937

938 **Table 1** ^{1}H (500 MHz) and ^{13}C NMR (125 MHz) data of compound **1** ($CDCl_3$)

No.	δ_C	δ_H
1	36.0	2.23, m; 1.84*
2	19.3	1.84*; 1.52, m
3	37.8	2.19, br.d (13.9); 1.04, ddd (13.9, 13.9, 4.5)
4	43.7	
5	53.3	1.40, d (12.2)
6	20.5	2.00, m; 1.85, m
7	32.0	2.10, m; 1.90, m
8	134.7	
9	133.3	
10	38.2	
11	66.9	4.30, dd (2.5, 2.5)
12	40.1	1.71, dd (11.6, 3.5); 1.30, dd (11.6, 3.5)
13	27.6	
14	44.3	1.81, m, 2H
15	40.9	1.50, m; 1.19, m
16	58.5	3.61, ddd (13.1, 11.4, 3.1); 3.53, dd (11.4, 5.8)
17	31.8	0.92, s
18	28.7	1.27, s
19	181.2	
20	18.2	0.85, s

* overlapped

939

940 **Table 2** ^{1}H (500 MHz) and ^{13}C NMR (125 MHz) data of compounds **2** and **3** (DMSO-d_6, *J* in Hz)

No.	**2**		**3**	
	δ_C	δ_H	δ_C	δ_H
1	36.7	1.75, m; 1.01, m	36.6	1.75, m; 1.03, m
2	19.3	1.74, m; 1.42, m	19.3	1.76 *; 1.41, m
3	37.3	2.02, m; 0.97, m	37.3	2.03, m; 0.99, m
4	42.9		42.9	
5	52.6	1.29, d (11.8)	52.6	1.29, d (11.5)
6	20.5	1.85 *; 1.72, m	20.5	1.86 *; 1.72, m
7	32.8	1.85*; 1.80, m	32.8	1.86 *; 1.81, m
8	124.8		124.8	
9	135.0		135.0	
10	37.7		37.7	
11	20.3	1.90, m; 1.83, m	20.4	1.90, m; 1.83, m
12	34.1	1.44, m; 1.17, m	34.0	1.45, m; 1.16, m
13	30.2		30.0	
14	43.8	1.65, d (17.9); 1.60 d (17.9)	43.9	1.65, d (18.0); 1.60 d (18.0)
15	36.2	1.47, m; 1.34, m	36.4	1.49, m; 1.36, m
16	63.2	3.67*; 3.32*	63.6	3.65, m; 3.32, m
17	27.2	0.89, s	27.2	0.87, s
18	28.3	1.15, s	28.3	1.13, s
19	178.9		178.6	
20	17.5	0.85, s	17.5	0.84, s
1'	99.8	4.55, brs	98.6	4.58, d (3.4)
2'	70.4	3.55, brs	71.9	3.16, dd (9.3, 3.4)
3'	71.1	3.43*	73.3	3.37, t (9.3)
4'	67.0	3.36, t (9.3)	70.3	3.05, t (9.3)
5'	74.1	3.28, m	72.8	3.33*
6'	61.3	3.64, dd (11.6, 2.1); 3.44, dd (11.6, 6.3)	61.0	3.60, brd (11.4); 3.43, dd (11.6, 3.0)

* overlapped

941

942

943 **Table 3** ^{1}H (500 MHz) and ^{13}C NMR (125 MHz) data of compound **4** (DMSO-d_6, *J* in Hz)

Amino acid	No.	δ_C	δ_H
L–	CO	171.4	
phenylalanine	*α*	54.2	4.37, dd (15.5, 7.9)
	β	36.6	2.84, m
	γ	137.5	
	ortho	129.2	7.17, m
	meta	128.0	7.24, m
	para	126.2	7.24, m
	NH		8.42, d (7.9)
L–valine	CO	170.5	
	α	58.2	3.83, t (9.2)
	β	26.1	1.94, m
	γ	19.7	0.81, d (6.2)
		18.4	0.62, d (6.6)
	NH		8.35, d (9.2)
D–isoleucine	CO	170.2	
	α	55.7	4.19, dd (8.5, 7.1)
	β	37.8	1.52, m
	γ	25.6	1.27, m; 1.01, m
	σ	11.5	0.83, d (6.2)
	β–CH_3	14.4	0.72, d (6.9)
	NH		7.07, d (8.5)
L–leucine	CO	168.8	
	α	47.6	4.61, dd (14.5, 8.6)
	β	41.5	1.51, m; 1.41, m
	γ	24.4	1.35, m
	σ	22.7	0.84, d (6.3)
		22.4	0.84, d (6.2)
	NH		8.34, d (8.6)
L–proline	CO	170.4	
	α	59.9	4.67, d (7.8)
	β	32.0	1.94, m; 1.61, m
	γ	20.9	1.65, m; 1.41, m
	σ	45.6	3.28, m

944

945

946 **Table 4** ^{1}H (500 MHz) and ^{13}C NMR (125 MHz) data of compounds **5**–**9** (*J* in Hz)

No.	**5**[a]	**6**[b]	**7**[b]	**8**[b]	**9**[b]
2	7.99, brs	7.79, brs	7.72, brs	7.71, brs	7.69, d (5.7)
3					6.30, d (5.7)
5	4.83, d (2.2)	4.59, d (7.7)	4.51, d (1.7)	4.27, d (7.6)	4.57, d (7.7)
6	1.37, m	1.64, m	1.32, m	1.97, m	1.63, m
7	1.77, m	2.03, m;	1.81, ddd (12.9,	2.15, m;	2.03, m;
		1.45, m	12.2, 6.7); 1.72, m	1.75, m	1.46, m
8	2.66, m	2.66, m;	2.63, dd (18.6, 6.7);	2.48, m	2.64, m;
		2.55, m	2.56, dd (11.4, 7.0)		2.54, dt (18.2, 4.8)
9	4.31, d (13.7);	4.33, d (13.5);	4.34, d (13.0);	4.35, d (13.6);	
	4.27, d (13.7)	4.29, d (13.5)	4.30, d (13.0)	4.27, d (13.6)	
10	1.63, m;	1.85, m;	1.64, m;	1.21, m;	1.84, m;
	1.41, m	1.28, m	1.44, m	1.13, m	1.28, m
11	1.04, t (7.3)	0.98, t (7.3)	1.00, t (7.4)	0.97, t (7.4)	0.98, t (7.5)
12	3.40, s	3.44, s	3.44, s	3.44, s	
13			3.54, s	3.54, s	

[a] CD_3OD; [b] $CDCl_3$

947

948 **Table 5** ^{13}C NMR (125 MHz) data of compounds **5**–**13**

No.	**5**[a]	**6**[b]	**7**[b]	**8**[b]	**9**[b]	**10**[b]	**11**[b]	**12**[b]	**13**[b]
2	155.2	152.8	152	152	155	151.3	153.5	152.6	152.7
3	126.0	125.2	125.3	125.4	116.5	125.5	121.4	125.2	125.1
4	179.2	179.5	177.6	177.6	180.3	174.5	177.2	178.2	178.6
4a	125.2	123.5	123.6	121.0	125.0	120.1	123.8	123.5	122.1
5	62.3	69.0	70.8	73.4	69.0	111.4	124.0	64.3	68.8
6	42.0	41.5	41.2	36.4	41.4	140.4	141.5	42.3	72.4
7	22.7	23.3	21.8	19.8	23.3	26.9	134.0	21.6	27.9
8	28.8	27.0	27.9	23.3	27.0	26.2	118.1	27.2	24.8
8a	168.8	165.6	166.6	166.0	165.7	162.4	155.1	165.6	165.6
9	67.0	66.1	66.5	66.5		66.6	66.6	66.2	66.2
10	25.3	25.3	24.6	22.0	24.5	29.8	28.5	138.2	29.3
11	11.9	11.3	12.1	12.2	11.3	12.1	15.7	116.1	6.8
12	58.9	59.2	59.1	59.2		59.1	59.0	59.2	59.2
13			60.2	58.1					

[a] CD_3OD; [b] $CDCl_3$

949

950

951 **Table 6** ^{1}H (500 MHz) data of compounds **10**–**13** ($CDCl_3$, *J* in Hz)

No.	10	11	12	13
2	7.71, s	7.95, s	7.78, s	7.78, s
5	6.37, s	8.03, d (2.2)	4.93, brs	4.62, s
6	/	/	2.39, m	/
7	2.39, t (9.2);	7.51, dd	2.05, m;	1.96, m;
	2.75, t (9.2)	(8.6, 2.2)	1.85, m	1.80, m
8	2.75, t (9.2)	7.38, d (8.6)	2.67, dd (6.0, 3.4);	2.81, m;
			2.62, dd (10.3, 6.2)	2.51, m
9	4.34, brs	4.43, d (1.0)	4.33, brd (13.5);	4.33, brd (13.6);
			4.29, brd (13.5)	4.29, brd (13.6)
10	2.17, dd	2.75, q (7.6)	6.08, m	1.89, m;
	(7.3, 7.1)			1.58, m
11	1.09, t (7.4)	1.28, t (7.6)	5.22, dd (1.3,1.3);	1.04, t (7.5)
			5.19, dd (5.3, 1.3)	
12	3.46, s	3.48, s	3.46, s	3.45, s

952

953 **Table 7** ^{1}H (500 MHz) and ^{13}C NMR (125 MHz) data of compound **14** ($CDCl_3$, *J* in Hz)

No.	δ_C	δ_H
1	162.1	
3	76.3	4.55, m
4	31.5	2.90, dd (16.1, 2.9);
		3.06, dd (16.1, 11.6)
4a	141.7	
5	119.5	6.82, d (8.0)
6	134.7	7.46, dd (8.0, 8.0)
7	111.1	6.92, d (8.0)
8	161.4	
8a	114.8	
9	73.6	3.62, dd (10.3, 5.4);
		3.70, dd (10.3, 4.9)
10	59.7	3.44, s
11	56.3	3.94, s

954

955

956 **Table 8** IC_{50} values of compounds **10**, **11**, **32**, **36**, and **41** against the induced proliferation of induced-T and
957 B lymphocytes, and their CC_{50} values for lymphocytes

Sample	T cells	B cells	lymphocytes
	IC_{50} (μM)		CC_{50} (μM)
10	>20	8.0	>20
11	>20	20.0	>20
32	3.1	6.0	>20
36	>20	16.7	>20
41	12.1	16.7	>20
Dex	1.9	1.0	0.2

958 **Table 9.** Inhibition rates of compounds **1**−**3** and **15**−**17** against the cell proliferation of ConA-induced T
959 lymphocytes and LPS-induced B lymphocytes, and cell validity treated with these compounds

Group	*c* (μM)	Inhibition rate (%)		Cell validity (%)	Group	*c* (μM)	Inhibition rate (%)		Cell validity (%)
		T	B				T	B	
1	40	16.5±1.5	20.4±6.3	90.7±4.0	**15**	40	28.8±5.8	29.0±12.2	80.2±1.8
	20	11.4±6.4	18.9±7.5	86.3±2.1		20	26.4±6.3	23.0±4.3	89.9±7.5
2	40	32.8±6.8	30.6±6.2	89.8±7.9	**16**	40	20.7±4.3	20.5±10.6	96.2±1.1
	20	23.8±0.9	24.9±8.6	100.0±2.4		20	13.1±2.7	19.3±4.6	101.8±6.9
3	40	26.5±3.3	22.6±9.6	89.9±4.4	**17**	40	16.3±4.3	20.7±6.9	100.0±8.5
	20	15.7±7.9	11.0±4.9	87.7±7.4		20	10.1±4.4	11.5±3.1	94.0±5.6
Dex	2	45.2±4.9	68.6±1.5	36.9±2.2	Con				100±9.5

960 **Table 10.** IC_{50} values of active compounds against the proliferation of HaCaT cells

Sample	IC_{50} (μM)	Sample	IC_{50} (μM)
9	35.0±3.1	**33**	33.9±2.8
10	30.9±2.7	**34**	32.2±3.4
13	31.1±2.6	**35**	31.5±2.4
19	29.70±3.3	**37**	32.0±2.2
22	32.3±1.5	**38**	25.2±1.6
24	32.5±2.0	**39**	32.6±3.6
25	35.1±1.9	**40**	32.9±3.4
28	29.1±1.7	**41**	27.7±2.5
30	31.2±4.1	MTX	26.4±1.4
32	27.0±1.3		

961